Article:
Wang, Y, Cai, G, Li, Y et al. (2019) Behavior of Circular Fiber-Reinforced Polymer–Steel-Confined Concrete Columns Subjected to Reversed Cyclic Loads: Experimental Studies and Finite-Element Analysis. Journal of Structural Engineering, 145 (9). 04019085. ISSN: 0733-9445

https://doi.org/10.1061/(ASCE)ST.1943-541X.0002373

Behaviour of Circular FRP-Steel Confined Concrete Columns Subjected to Reversed Cyclic Loads: Experimental Studies and FE Analysis

Yanlei Wang[1], Gaochuang Cai[2]*, Yunyu Li[3], Danièle Waldmann[4], Amir Si Larbi[5], Konstantinos Daniel Tsavdaridis[6]

Abstract

This paper studies experimentally the behaviour of circular FRP-steel confined concrete columns subjected to reversed cyclic loads. The influence of main structural factors on the cyclic behaviour of the columns is discussed. Test results show the outstanding seismic performance of FRP-steel confined reinforced concrete (RC) and steel-reinforced concrete (SRC) columns. The lateral confinement effectiveness of GFRP tube and GFRP-steel tube was verified and a simplified OpenSees-based finite element method (FEM) model was developed to simulate the experimental results of the test columns. Based on the proposed FEM model, a parametric analysis was conducted for investigating the effects of main factors on the reversed cyclic behaviour of GFRP-steel confined RC columns. Based on the test and numerical analyses, the study discussed the influence of variables such as the lateral confinement on the plastic hinge region (PHR) height and peak drift ratio of the columns under reversed cyclic loads. Results indicate that the lateral confinement significantly affects the PHR height of the circular confined RC columns. Based on the analyses of the data from this study and literature, a simple model was suggested to predict the peak drift ratio of the confined RC columns.

[1] Associate professor, State Key Laboratory of Coastal and Offshore Engineering, School of Civil Engineering, Dalian University of technology, Dalian 116024, China.
[2] Invited professor, Univ Lyon, Ecole Nationale d'Ingénieurs de Saint-Etienne (ENISE), Laboratoire de Tribologie et de Dynamique des Systèmes, UMR 5513, 58 Rue Jean Parot, 42023 Saint-Etienne Cedex 2, France ; Assistant professor,Faculty of Engineering, Fukuoka University, Fukuoka, Japan. *(Corresponding author), Email: gaochuang.cai@enise.fr;*
[3] Lecturer, School of Transportation, Wuhan University of Technology, Wuhan 430063, China.
[4] Associate professor, Laboratory of Solid Structures, University of Luxembourg, Maison du Nombre, 6, Avenue de la Fonte, L-4364 Esch-sur-Alzette, Luxembourg.
[5] Full Professor, Univ Lyon, Ecole Nationale d'Ingénieurs de Saint-Etienne (ENISE), Laboratoire de Tribologie et de Dynamique des Systèmes, UMR 5513, 58 Rue Jean Parot, 42023 Saint-Etienne Cedex 2, France.
[6] Associate professor, School of Civil Engineering, University of Leeds, Woodhouse Lane, Leeds, LS2 9JT, UK.

Keywords: Seismic behaviour; FRP; Lateral confinement; Plastic hinge region; composite structure; Hysteresis behaviour

1. Introduction

It is generally accepted that properly confined concrete can develop adequate ductility for reinforced concrete (RC) elements allowing sufficient lateral deformability without a significant reduction in strength. For RC beams and columns, their confinement is usually located at the plastic hinge regions (PHR) by using different external constraints such as steel tube (Tomii 1985a, 1985b) and fibre reinforced polymer (FRP) sheet (Teng et al. 2002). Moreover, the confinement can further enhance the deformability and ductility of RC columns subjected to reversed cyclic loads, which is meaningful for concrete structures in seismic regions or for high-rise buildings. This is because that unconfined concrete elements might fail due to damage accumulation during reversed cyclic loads, thus leading to subsequent further damage or the collapse of whole structure.

Fig.1 shows the main confinement methods of two kinds of concrete elements: (i) RC, and (ii) concrete-filled steel tube (CFST) elements. For the former, the addition of external steel tube confinement was suggested to improve the ductility, deformation, and damage control of the concrete cover of RC elements. The concept of "tubed column" was first introduced to the research community by Tomii et al (1985a,b), which is called as steel tube confined columns. The lateral tubed confinement at the same time significantly enhances the bearing capacity of the RC elements. Additionally, the external steel tube can work as a part of the formwork system to quicken the construction. Since steel tube confined concrete (STCC) elements initially were used in the construction industry and presents excellent deformation ability and ductility, the research community has also presented increasing concerns. This can be attributed to the fact that the STCC effectively avoids the outward local buckling (OLB) for the local yielding of the steel tube under large loads or at large lateral deformation (Tomii et al. 1985a, 1985b, Sakino *et al.* 2004), which usually occurs in CFST elements. This is also because the steel tube is designed not to carry directly axial loads in STCC elements via the termination of the steel tube at its two ends. Besides, the STCCs provide a

solution to overcome the difficulty of the load transfer mechanisms and the detailing design at RC beam-to-CFST column joint nowadays. Up-to-date, a number of studies have been conducted to understand the constitutive behaviour (Binici 2005, Li *et al.* 2005) and structural behaviour of STCCs under various loads (Aboutaha and Machado 1999). In particular, Han *et al.* (2005) experimentally investigated the monotonic and cyclic behaviours of STCC columns, thin-walled STCC column to beam joints (Han *et al.* 2009), and thin-walled STCC columns subjected to axial local compression (Han *et al.* 2008). Zhou and Liu (2010) experimentally studied the seismic behaviour and shear strength of STCC short columns, the performance of STCC columns under eccentric compression (Zhou *et al.* 2015, Zhou *et al.* 2016), the behaviour of circle STCC column-to-RC beam connections under axial compression (Zhou *et al.* 2017). In addition, Yu *et al.* (2010) proposed a finite element method (FEM) analysis model to analyse the mechanisms of STCC columns under axial compression.

However, similar to the buckling of the steel tube in CFSTs at large deformation and its corrosion under aggressive environment limit their application in civil engineering, the corrosion of the steel tube also obstructs the application of the STCCs in an increasing deteriorative built environment. According to literature (Wu *et al.* 2014, Liu *et al.* 2018), the FRP wrapping of the STCC solves the durability concerns of the STCC structures. However, a few concerns regarding this kind of structural elements still need to be addressed such as low longitudinal stiffness and relatively high construction cost. Therefore, with consideration of these reasons, a FRP-steel confined RC element has been developed. The first author's research group (Ran 2014, Huang 2016) investigated the constitutive behaviour of GFRP-STCC under monotonic and cyclic axial loads. Cao *et al.* (2017) experimentally investigated the behaviour of FRP-STCC stub columns with expansive self-consolidating concrete under axial compression. Liu *et al.* (2018) studied the axial behaviour of circular CFRP-STCC stub columns. In summary, comparing with STCC and FRP-confined concrete structures, the FRP-STCC structures are more durable and flexible because of the using of durable FRP materials and a more effective confinement.

On the other hand, CFST elements are popular in high-rise buildings or piers in Europe and Japan as reinforced concrete is widely applied. This is due to the reasonable arrangement of steel and concrete in the section, which optimizes the sectional strength and stiffness of the elements leading to an effective use of the material properties to resist the tension and bending actions in the section. Meanwhile, the tube can serve as a part of formwork in construction, which decreases labour and material costs. However, the effects of the bond, confinement, and OLB on CFST's structural behaviour are under study to facilitate the development of design methods of the members under lateral reversed cyclic loads. External FRP confining may be a potential solution to fix the OLB problem of CFST elements (Xiao 2004, Hu *et al.* 2011) for the high strength and elastic properties of FRP materials, but which is still under research. Xiao (2004) proposed the FRP-confined CFST columns, who also compared and commented the FRP-STCC and CFST elements. He concluded that a FRP-confined CFST column combines the advantages of the conventional CFST column and the tubed column, in which additional transverse reinforcement is designed for the potential plastic hinge regions to improve the seismic performance of the elements. In 2005, Xiao *et al.* (2005) performed a study to introduce and experimentally validate FRP-confined CFST columns under axial and seismic loads and confirmed the excellent seismic performance of these columns. Recently, several studies were reported to examine the constitutive behaviour of FRP-confined CFST columns (Xiao *et al.* 2005, Liu and Lu 2010, Park *et al.* 2010, Tao *et al.* 2011, Lin 2012, Teng *et al.* 2013, Park and Choi 2013, Hu and Seracino 2013, Wang *et al.* 2015,Yu *et al.* 2016), but more studies are underway to examine details of the elements.

Concerning the structural behaviour of FRP-STCC elements under various loads, up to present, there are only limited studies available in literature. Most of the studies focused on the behaviour of the elements under axial compressive loads (Cao *et al.* 2017, Liu *et al.* 2018). Therefore, the major objective of this paper is to study the behaviour of circular GFRP-STCC columns under combined constant axial loads and lateral reversed cyclic loads. Based on experimental observations and analyses of the deformation mechanisms, this paper also proposes a FEM analysis model to simulate the structural response under the combined loads. Moreover, this study also aims to discuss the effect

of the main structural design factors on the behaviour of FRP-STCC columns under reversed cyclic loads.

2. Experimental program

2.1 Test overview

In this experiment, eight circular sectional concrete columns were designed and prepared, including one reinforced concrete (RC) column, one steel tube-confined RC column, one steel tube-confined steel reinforced concrete (SRC) column, one CFRP-steel confined RC column, two GFRP-steel confined RC columns and two GFRP-steel confined SRC columns. The core concrete diameter of all specimens was 300 mm and the thickness of the concrete cover was 30 mm. The height of the columns was 1350 mm with a 300 mm high column head. The dimension details and steel arrangement of the specimens are presented in Fig. 2. The volumetric ratio of longitudinal steel bar of all specimens was 1.71%, and the stirrup volumetric ratio was 0.6%. For the steel tubes confined specimens, the thickness of the steel tubes was 3.0 mm. In order to prevent the direct axial compression of the steel tubes, 20 mm gaps were set at both ends of the columns. In FRP confined specimens, FRP was used to confine the hinge zone of 500 mm with different layers depending on the test design, while the remaining parts of the columns were wrapped by 2-layers same-type FRP sheet. For the confined SRC columns, a standard H-section steel (150mm×150mm×10mm×7mm) was set from underneath the base beam to the top of the column. Table 1 and Fig.2 (a) show the details of test specimens.

2.2 Specimen manufacture

All steel tubes in the study were manufactured from 3.0 mm steel plates by welding at their lap zone. The tested specimens were prepared following the steps: (1) setting of the reinforcement cage of columns and base beam; (2) setting of the steel tube (its welding line was placed on the plane oriented parallel to the column's axis of symmetry); (3) setting of the reinforcement cage and module of the stigma (column head); (4) curing of the specimens; and (5) removing steel tube for concrete columns or wrapping FRP sheet for FRP-steel confined concrete columns. The key steps of FRP wrapping were as follows: (1) polishing their surface with an angle grinder to enhance its surface roughness;

(2) clearing the surface of the steel tubes such as wiping them with alcohol; and (3) setting of FRP sheet. The overlap length of FRP wrapping was about 300 mm and the welding line of the steel tube was located in the middle of the overlap zone of FRP wrapping to prevent the cracking of welding line. Fig. 2(b) shows a completely GFRP-steel confined column specimen.

2.3 Materials' properties

Two kinds of unidirectional FRP sheets were used, i.e. GFRP sheet L900 (900 g/m^2) and CFRP sheet UT70-30 (300 g/m^2). A construction impregnation adhesive for structural application, an epoxy adhesive Lica-100 was used, whose properties are listed in Table 2. Ready-mixed concretes were used, which contained 5-10mm aggregates with a target compressive strength of 40 MPa. According to the test results of six standard concrete cubes (150mm×150mm×150mm), the cube compressive strength of concrete was 41.2 MPa, which is approximately transferred as a concrete cylinder' compressive strength via multiplying by 0.8 for normal strength concrete. The transverse and longitudinal reinforcements of the columns are 8mm plain (smooth) steel rebars and 16mm deformed steel rebars, respectively. Q235 steel tube (3.0 mm thickness) was used to confine the columns, whose properties are listed in Table 2 obtained by the standard test method, GB/T228-2010 (2009). As shown in Fig. 2, a standard H-section steel (150mm×150mm×10mm×7mm) was used in the tested SRC columns.

2.4 Test setup and measurement

The details of the test setup are illustrated in Fig. 3. The bottom base beam of each specimen was firstly anchored on a strong RC floor through several high strength steel bolts. At the ends of the beam, two linear variable differential transducers (LVDTs) were used to record its possible slipping during the test. The constant axial loads were applied on the top of the columns by a hydraulic jack with a maximum capacity of 1000 kN, as shown in Fig. 3. The reversed lateral cyclic load was applied at the column head using a hydraulic jack with a maximum capacity of 1000 kN with a one-way steel hinge device that can rotate around the vertical and horizontal loading directions. The applied axial load in each column was designed as 978 kN for RC columns and 1242 kN for SRC columns - about

35% of the nominal axial load capacity (N) of the columns obtained as per the Chinese standards (GB 50010-2010 2015, TGJ3-2002 2002).

During the tests, the lateral load and displacement of the columns were monitored by using one load cell and several LVDTs (450 mm, 600 mm, and 750 mm from the top of the base beam), while the strains of the longitudinal reinforcement, the stirrup, FRP-steel tube and steel tube during the loading were investigated through several gauges. Four strain gauges (L1~L4) and three hoop strain gauges (H1~H3) were installed on the longitudinal rebars and on the stirrups at a distance of about 10mm from the top of the base beam, respectively. Two hoop strain gauges (HN, HS) and three vertical strain gauges (LN, LS, and LM) were arranged respectively on the surface of the steel tube or the FRP tube at the distances of 70 mm, 220 mm, and 370 mm from the top of the base beam, in order to measure the horizontal and vertical strains of the steel tube or the FRP tube.

2.5 Loading methods

It is necessary to establish a reasonable loading history to capture the critical issues of the resistance and deformation on structural elements during the quasi-static cyclic loading tests. After the application of a constant axial load on top of the columns, a multiple reversed cyclic lateral loading was performed in each column. In the reference column, a deformation-controlled reversed cyclic lateral loading was applied with an increment of 4.0 mm. The target deformation of the first cyclic loading was 4.0 mm. When the lateral displacement arrived at 12mm, the lateral loading was repeated twice at each target cycle of lateral loading. A similar loading method was performed at the confined concrete columns, except for that the increment of lateral deformation was set as 8.0 mm after the lateral displacement of the columns excessed 16mm. For the security, the tests were finished if the lateral resistance force of the specimen reduced to 60% of its maximum measured value or the lateral displacement of the columns is too large such as over 100mm. Fig. 4 presents the loading procedure applied in the columns.

3. Test observations

3.1 Cracking evolution and damages

(1) RC column and steel tube confined RC column (G0S0T0 and G0S1T0)

In Specimen G0S0T0, the first horizontal crack occurred at the north side of the column about 100 mm from the top of the base beam. Then, a semi-circular horizontal crack appeared on the south side with a height of 100 mm. At the same time, a second crack appeared at a north side of the column, at a height of 200 mm. Meanwhile, horizontal cracks began to appear in the upper part and in the middle of the south side and began to develop to the north side of the column. Next, new horizontal cracks appeared in the columns about 400 mm and 600 mm from the top of the base beam. With the increase of the lateral displacements, the cracks below the south side developed, while the horizontal cracks continued to develop, and crushing of the concrete at the south side of columns occurred. At this time, the first vertical crack was confirmed in the south side concrete along with the crushing of the concrete on the north side. Next, at the north side of the concrete first vertical cracks appeared. When the lateral displacement was about 24 mm, the concrete cover on the north side shows a large area of spalling but a buckling of the longitudinal reinforcing bar could not be observed. All the damages and cracks in the column were mainly caused by the plastic deformation of concrete and internal damage surrounding the deformed reinforcements. The final failure morphology of the specimen is shown in Fig. 5.

In the steel tube confined RC column, G0S1T0, the early stage cracks cannot be visually observed due to the external steel tube. When the lateral displacement was 48mm, the cracking and the extrusion exfoliation of concrete were found at the bottom of the column. After removing the steel tube at the end of the column, the concrete at the bottom of the confined zone was crushed, but due to the constraints of the steel tube, it did not fall off. Several slipped shear cracks were also found at the foot of the column. All of damages and cracks were still caused by the plastic deformation of the elements, however, the confinement of steel tube effectively reduces the crushing of the concrete which indicates the failure of the column will be difference with that of RC columns in which the sectional concrete crushing is one of main reasons of structural failure.

(2) FRP-steel confined RC columns (G5S1T0, G7S1T0 and C7S1T0)

Specimen G5S1T0 presented a large residual displacement after testing. At the surface of GFRP tube wrapped in the column foot, the resin slightly cracked. After removing of the GFRP wrapping and steel tube, several cracks were found at the column foot and the south side of the column. This can be explained by the fact that the compression from the upper part of the north side GFRP-steel confined concrete promotes the crushing to the below concrete (about 50 mm from the top of the base beam). However, the damage of the outermost layer of GFRP tube did not appear during testing. Compared to Specimen G5S1T0, two more layers of GFRP sheets were applied in Specimen G7S1T0, but the failure mode of the two specimens is similar. When the lateral displacement was too large, the concrete at the top of the base beam was disintegrated. By removing the GFRP tube and steel tube after testing, several horizontal and diagonal cracks were observed at the distance of 100 mm from the top of the base beam. However, the confinement of the GFRP was able to protect the core concrete in a satisfactory manner. Comparing with Specimen G7S1T0, when GFRP was replaced by CFRP, similar failure mode, cracking pattern, and damages were found in Specimen C7S1T0, so that it can be stated that the confinement of the columns were performant. In summary, the main damages and cracks of FRP-steel confined RC columns concentrated on the critical section between the column and the base beam, which were expressed as crushing and slipped cracks, respectively.

(3) FRP-steel confined SRC columns (G0S1T1, G5S1T1 and G7S1T1)

The cracks and damages of the steel tube confined SRC column G0S1T1 were similar to that of the steel tube confined RC column G0S1T0. When the lateral displacement increased to about 48mm, the parts of the concrete on the top of the base beam and the column foot were cracked and damaged as the steel tube deformation and stretched continuously. At the end of the test, there was no apparent buckling or other failure characteristics visible on the steel tube. When removing the steel tube later, a horizontal crack was observed at about 80 mm near the column foot but no other damages to the column body. When the steel tube was confined by GFRP tube such as Specimen G5S1T1, the cracks appeared on the south side of the column above the base beam when the lateral displacement of the column was 25mm. These cracks developed further into compressive damage of the concrete cover.

231 At the end of the experiment, however, the confined concrete is still almost intact. Comparing with
232 the case of Specimen G5S1T1, the cracks and damages were controlled well when using more layers
233 of GFRP sheets in G7S1T1. However, the failure mode of this specimen was similar to that of
234 Specimen G5S1T1. In the case of large displacement, the concrete at the top of the base beam was
235 initially disintegrated, before being damaged near the top of the column. At last, the concrete was
236 damaged at around 10 mm over the base beam, while the confined concrete remained protected
237 without visual horizontal or diagonal cracks. In summary, the damages and cracks in the confined
238 SRC columns were much smaller than those of the other columns, which is attributed to the
239 reinforcement of the strong H-sectional steel inside.

240 ## 3.2 Hysteresis behaviour

241 **(1) RC and steel tube confined RC columns (G0S0T0 and G0S1T0)**

242 Regarding the RC column, the lateral load-displacement curve is almost linear at the initial stage of
243 loading. At the second cycle of the same target deformation, the stiffness and lateral load-bearing
244 capacity of the specimen hardly degraded. However, the residual deformation became larger and the
245 unloading stiffness and bearing capacity decreased with the increase of the lateral displacement, but
246 the pinch contraction phenomenon of the hysteresis hoops was not obvious. When the displacement
247 was 24 mm, the test was stopped due to the large area of concrete spalling. At this moment, the lateral
248 load was 73.4% of the axial peak load of the column. For specimen G0S1T0, the residual deformation
249 during unloading was small at the beginning. The stiffness and the bearing capacity of the specimen
250 at the early stage are not significantly decreased at the same deformation level. As shown in Fig. 6,
251 the hysteretic pinch phenomenon was also not obvious in this column showing that it has a strong
252 energy dissipation capacity. When the lateral displacement was 72mm, the lateral load decreased to
253 62% of its peak load.

254 **(2) FRP-steel confined RC columns (G5S1T0, G7S1T0 and C7S1T0)**

255 Regarding specimen G5S1T0, the lateral load and stiffness of the specimen have not changed and its
256 residual deformation was small at the initial stage. However, as shown in Fig. 6, with the increase of

lateral displacement, the hysteresis loop appears an obvious pinch and shrink phenomenon, but the shape of the loop is still fat. The bearing capacity of the column did not decrease rapidly after reaching the peak load indicating that the ductility of the column was satisfactory. For specimen G7S1T0, the shape and variation of the hysteresis curve were very similar to that of G5S1T0, however, the hysteresis loop of the G7S1T0 was fatter. For specimen C7S1T0, its residual deformation was small while the stiffness and bearing capacity had almost no degradation when the displacement was small. As the displacement increased, the residual deformation of the specimen increased, and the stiffness and bearing capacity decreased obviously.

(3) FRP-steel confined SRC columns (G0S1T1, G5S1T1 and G7S1T1)

As it can be seen from Fig. 6, G0S1T1 specimen shows a fusiform hysteresis loop at the initial stage, while the hysteresis curve is gradually getting fatter with the increase of the displacement and shows no sign for the pinch-and-shrink phenomenon. This demonstrates that the column possesses an excellent energy dissipation ability. For specimen G5S1T1, its bearing capacity and stiffness did not significantly change under the same displacement. With the increase of loading, the shape of the hysteresis loop tended to become fatter. The degradation rate of the lateral load was small after the column reached its peak load meaning that the column has a satisfactory ductility. For specimen G7S1T1, the residual deformation of the column during the initial loading was quite small. Similar to that of G5S1T1, no obvious degradation occurred in the stiffness and lateral load of the specimen at the same level of lateral displacement. With the increase of lateral displacement largely, the hysteresis curve of the specimen become fatter showing its strong energy dissipation capacity. Comparing between G7S1T1 and G5S1T1, no significant difference was observed in G7S1T1 indicating that increasing the number of GFRP layers has no influence on the seismic performance of the SRC columns.

3.3 Strain evolution of reinforcing rebars and steel tube

Fig. 7 demonstrates that when the lateral load increases, the strain of the steel rebars increases as the lateral displacement of RC column and steel tube confined RC columns. When the displacement was

283 32 mm, the longitudinal reinforcement in L2 has a strain of higher than its yielding strain, i.e. 2000με.
284 With the increase of the lateral displacement, the longitudinal reinforcement begins to yield. However,
285 the maximum compression strain of the longitudinal reinforcement reached 2500με at the later
286 loading stage indicating that it did not undergo significant plastic deformation. The figure shows that
287 the stirrups can confine the concrete well in the circular RC column.

288 As shown in Fig. 7, taking specimen G7S1T0 as an example with the FRP-steel confined RC columns,
289 the maximum strains of the steel tube occurred at the top of the base beam in both sides are 6602με
290 and 3543με - both exceeding the yielding strain of the tube. The hoop strain on the outside tube
291 confirmed that the steel tube were in tensile. Similar to the variation law of longitudinal strain, the
292 amplitudes of HN50 and HS50 close to the top of the base beam were 4883με and 4883με,
293 respectively. Specimen G0S1T1 shown a similar strain evolution to Specimen G7S1T0. For FRP-
294 steel confined SRC column G5S1T1, the strains of LN50 and LS50 near the base beam were 6823με
295 and 5949με, respectively. All the results of strain gauges indicated the steel hoop were under tension.
296 This is due to the expansion of the core concrete after multiple lateral reserved loads leading to an
297 increase in the deformation of steel tube confined by GFRP sheet. At the same time, HN50 and HS50
298 located on the south and north sides were 6755με and 4799με, respectively which reached its yielding
299 status. In summary, in the FRP-steel confined SRC columns, at the same section of the column foot,
300 the strain on the north side, the south side, and the neutral axis were all different, which means that
301 the hoop strain distribution was not uniform. The strain of the steel tube in the confined SRC columns
302 was smaller than that of other specimens because the sectional rigidity of the SRC column is quite
303 large for the using of H-section steel.

304 ## 4. Comparison and analyses

305 ### 4.1 Comparison of hysteresis behaviour

306 Fig. 8 compares the hysteresis curves of all the tested specimens. Results show that the bearing
307 capacity and ductility behaviour of specimen G0S1T0 was better than that of the specimen G0S0T0

owing to the external lateral confinement of steel tube. Comparing to Specimen G0S1T0, an overall improved bearing capacity, ductility, and energy dissipation capacity of the steel tube confined RC column was obtained by the GFRP wrapping, such as the specimens G5S1T0 and G7S1T0. Furthermore, with the increase of the number of layers of FRP sheet, the enhancement effect of GFRP wrapping was more obvious.

Examining the case of the specimens G5S1T0 and G7S1T0, the seismic performance of the FRP-steel confined RC columns was improved with the number of layers of FRP sheet, but the enhancement effectiveness became lower with the number of FRP layers. For the specimens G7S1T0 and C7S1T0, although the lateral confinement (both the lateral confinement stiffness and strength) of the CFRP was stronger than that of the GFRP, the load-carrying of the specimen G7S1T0 is slightly better than the specimen C7S1T0. This can be explained as follows: (a) the failure mode of the confined RC columns was controlled by the damages and cracks in the confined RC, but not controlled by the rupture of the FRP wrapping usually occurred in axial compressive columns, which indicated that the FRP material were not fully utilized; (b) this little abnormal case may be induced by the manufacture error of the specimens, and testing error etc.

For GFRP-steel confined RC/SRC columns, it was observed that the bearing and deformation capacities of the specimen G5S1T1 (or G5S1T0) were improved when using GFRP to confine steel tube, comparing with the ones of specimen G0S1T1 (or G0S1T0). This indicates that the FRP-steel composite tube can improve the seismic performance of the RC/SRC columns in an effective manner. However, when the used amount of steel reinforcement (H-section steel, steel reinforcing bars, and steel tube) was high, the improvement caused by FRP wrapping became not obvious. For the specimens G5S1T1 and G7S1T1, the increase of the number of layers of FRP did not improve significantly the shear-resistance and the deformation capacity of the confined SRC columns. This could be explained by the fact that the confined columns using H-section steel already have a high seismic performance indicating that the confinement effectiveness from FRP sheets was not developed.

4.2 Skeleton curves-deformation and ductility

Skeleton curves can clearly reflect the bearing capacity and ductility of RC members which are the main considerations of the seismic design of the members. Generally, a skeleton curve mainly includes three characteristic points: yield strength point, peak strength point, and ultimate strength point. The peak point is the peak load of the columns, P_{max}. For the FRP-steel confined RC columns, the ultimate point is the point at 85% of the peak load (85% P_{max}), P_u. The deformability of FRP-steel confined SRC columns was excellent; however, the ultimate deformation was large when the lateral load drop is not obvious. Due to safety reasons, all tests were stopped before reaching the ultimate state of the columns. For a comparative analysis, the ultimate strength points of two FRP-steel confined SRC columns (Specimens G5S1T1 and G7S1T1) were considered as a point when the lateral load drops to 90% of its peak load in this study.

There is no uniform the calculation method to adjust the yield point of the concrete element. In this paper, the equivalent elastoplastic energy absorption method (Park 1988) was applied to define the yielding point by introducing an additional line in the load-deformation curve such as to define an equivalent elastoplastic displacement with the same energy dissipating, as shown in Fig. 9: the trapezoidal OABC area is equal to the area encircled by the curve ODBCO. In this figure, Δ_u and P_u represent the ultimate displacement and the ultimate load, respectively; P_y and Δ_y are the yield load and displacement, respectively. P_{max} is the peak load and Δ_{max} is the corresponding displacement. P_u is taken as $85\%P_{max}$ or $90\%P_{max}$ depending on columns with/without H-section steel with the exception of Specimen G0S1T1 ($85\%P_{max}$). R is the drift angle of the columns.

Fig. 10 shows the comparison of the skeleton curves of all the tested specimens and Table 3 presents a summary of all test results. The yield loads of FRP-steel confined RC columns without H-section steel increased slightly with the number of layers of FRP wrapping. The yield displacement for the steel tube confined or FRP-steel confined RC columns was larger than that of RC columns. Compared to Specimen G0S1T0, G5S1T0 and G7S1T0 have a larger yield load which increased by 5.6% and 11.0%, respectively. The peak loads of the specimens G5S1T0 and G7S1T0 increased by 10.2% and 16.0%, respectively, while their peak displacements increased by 14.9% and 28.4%, respectively, and

their ductility coefficients increased by only 0.5% and 3.1%, respectively. This indicates that the ultimate shear capacity and deformation capacity of the steel tube confined RC column were significantly improved after confinement by FRP wrapping, while no significant improvement was achieved for its ductility. On the other hand, CFRP-steel confined specimen (C7S1T0) had a better ductile coefficient which was higher than that of GFRP-steel confined specimen (G7S1T0) because the confinement of the CFRP was stronger than that of the GFRP, as the same number of layers of FRP was used.

With regard to the specimens using H-section steel, similar results were obtained. Comparing to the specimens G0S1T1, with an increase of the number of GFRP layers, the yielding load of the specimens G5S1T1 and G7S1T1 increased slightly by 0.3% and 10.2%, their peak load increased by 8.8% and 17.9% and their ultimate displacement increased by 7.1% and 12.9%, respectively. Meanwhile, the ductility coefficients of the G5S1T1 and the G7S1T1 also increased slightly with increasing the number of GFRP layers.

4.3 Stiffness degradation

The lateral stiffness of RC columns generally degrades under a reversed cyclic loading for several reasons such as the decreasing of effective compression area of columns caused by concrete cracking and the yielding of steel reinforcement etc. The stiffness in this study refers to an equivalent lateral stiffness, which is the average value of the load-displacement ratios at the unloading points in the positive and negative directions of the first loading hoop of each target displacement level. Fig. 11 demonstrates the stiffness degradation curve of all specimens. Results show that the initial stiffness of the RC column (G0S0T0) is low, while the members confined by steel tube or FRP-steel tube have a much higher stiffness. As the lateral displacement increases, the stiffness of the confined RC columns degraded slowly. In addition, the stiffness degraded more slowly when the number of GFRP layers increased. The initial stiffness of specimens G0S1T1, G5S1T1, and G7S1T1 are almost the same due to all SRC columns have a strong stiffness. As the lateral displacement increased

continuously, the degradation rates of the lateral stiffness of the SRC specimens remained an almost identical value.

4.4 Energy dissipation capacity

The energy dissipation capacity of RC elements is an important index to evaluate their capacity to absorb earthquake energy induced by ground shaking. The failure and collapse of RC structures could happen due to poor energy dissipation during an earthquake. In this study, the cumulative energy dissipation was calculated considering only the first load hoop at the corresponding displacement level. As shown in Fig. 12, the accumulated energy dissipation of RC columns is less than that of the confined RC columns at the same lateral displacement. As the number of GFRP layers increased, the energy dissipation capacity of the confined columns increased. However, the accumulated energy dissipation of the G7S1T0 was only slightly higher than that of the G5S1T0. This is because the specimen G5S1T0 wrapped with 5 layers of GFRP may be already under an over-confining state. Therefore, the effect of increasing GFRP layers on energy dissipation may be small in G7S1T0. Similarly, the specimen C7S1T0 got a greatly improved energy dissipation capacity comparing to the specimen G0S0T0, but when comparing to the specimens G7S1T0 and G5S1T0, their energy consumption capacity was almost the same.

For the SRC columns (G0S1T1, G5S1T1, and G7S1T1), similar behaviour was obtained: (1) in the initial stage, the accumulated energy dissipation of the specimens was similar for all the specimens; (2) as the lateral displacement increased, the energy dissipation capacity of the columns increased and shown a different evolution and finally the energy consumption of the G7S1T1 is highest; and (3) the number of GFRP layers has no significant influence on the energy dissipation capacity of the SRC columns. This again shows that the improvement of the seismic performance of the SRC columns due to an increasing the number of layers of GFRP sheet is relatively small.

5. FEM simulation of FRP-steel confined RC columns

According to Section 4, the GFRP wrapping did not present its positive effect on the seismic performance of the SRC columns. The main reason could be that the core SRC column possessed

already a high stiffness to the lateral deformation under the reversed cyclic loads. Therefore, in this section, the paper emphasizes on the simulation of FRP-steel confined RC columns. OpenSees (Mazzoni et al. 2006), as an open source object-oriented software, is used for the analysis of the tested RC and FRP-steel confined RC columns. The basic assumptions for the analyses of the columns include: (a) concrete section remained a plane and normal to the neutral axis after bending, (b) the slippage between steel rebar and concrete was neglected to simplify the simulation, and (c) the shear effect was neglected to simplify the simulation due to the fact that the shear span ratios of all columns in this FEM is not less than 2 (especially most case is 4), which indicated the flexural failure mode will occur in the columns and the shear effect would be relatively small. In the following sections, the geometric and materials models used in the program are discussed.

5.1 Material model and cross-section rule

5.1.1 Concrete and steel tube confined concrete

For the RC column, a three-line constitutive model proposed first by Kent and Park (1971) and modified by Scoot *et al.* (1982) was selected as a backbone curve for concrete material. The backbone and hysteresis model of concrete (uniaxial materials of Concrete01 in OpenSees) are presented in Fig. 13 (Mazzoni et al. 2006). The related equations of the model are as follows:

$$f = \begin{cases} Kf_{co}\left[2\left(\dfrac{\varepsilon}{\varepsilon_{cc}}\right)-\left(\dfrac{\varepsilon}{\varepsilon_{cc}}\right)^2\right], \varepsilon \le \varepsilon_{cc} \\ Kf_{co}\left[1-Z\left(\dfrac{\varepsilon}{\varepsilon_{cc}}\right)\right], \varepsilon_{cc} \le \varepsilon \le \varepsilon_{cu} \\ 0.2Kf_{co}, \varepsilon \ge \varepsilon_{cu} \end{cases} \quad (1)$$

In the equation,

$$K = 1 + \rho_v f_{yh}/f_{co} \quad (2)$$

$$Z = \frac{0.5}{\frac{3+0.29f_{co}}{145f_{co}-1000} + 0.75\rho_v\sqrt{\frac{b}{s}} - 0.002K} \quad (3)$$

Where, ε_{cc} is the strain corresponding to the peak stress of the confined concrete, taken as $0.002K$; K is the coefficient of the increase of the peak load caused by the confinement. Z is the slope of the strain drop curve; f_{co} is the compressive strength of standard non-confined concrete cylinders; f_{yh} is the yield strength of stirrups; ρ_v is the volumetric reinforcement ratio of stirrups; b is the width of core concrete; s is the spacing of stirrup. For steel tube confined RC columns, the analysis of the confined concrete of the columns adopted the constitutive model of steel tube confined concrete proposed by Lin (2012).

5.1.2 FRP-steel confined concrete model

a. Monotonic model

An analysis-oriented stress-strain model for FRP-steel confined concrete was used in this paper. Referring to analysis-oriented models for FRP-confined concrete (Jiang et al. 2007), a passive confining stress-strain model for FRP confined concrete in FRP-steel confined concrete columns can be achieved from an active confining model for concrete through an incremental approach. The model is proposed on the assumption that the axial stress and strain of FRP confined concrete at a given hoop strain are the same as those of the same concrete confined actively with a constant confining pressure equalling to that provided by the FRP wrapping (Jiang et al. 2007). The following axial stress-strain model for concrete, which was built by Popovics (1973), is adopted in this paper. Popovics (1973) proposed a stress-strain model for the confined concrete with an active confining, which presents a great analysis accuracy. Thus, this study suggests to use it to analyse the stress-strain of GFRP-steel confined concrete elements, which is given as:

$$\frac{\sigma_c}{f_{co}} = \frac{(\varepsilon_c/\varepsilon_{cc})\cdot r}{r-1+(\varepsilon_c/\varepsilon_{cc})^r} \quad (4)$$

$$r = \frac{E_c}{E_c - f_{cc}/\varepsilon_{cc}} \quad (5)$$

Based on the research conducted by the research group of the first author of the paper (Lin 2012, Ran 2014, Huang 2016), the study suggests to consider the active (stirrups and steel tube) and passive confining actions (FRP wrapping) in FRP-steel confined concrete columns to model the peak axial stress and the corresponding axial strain of FRP-steel confined concrete. The proposed models are expressed as:

$$\frac{f_{cc}}{f_{co}} = 1 + 4.08\left(\frac{f_{lf}}{f_{co}}\right)^{1.28} + 5.5\left(\frac{f_{ls} + f_{lh}}{f_{co}}\right)^{0.86} \tag{6}$$

$$\frac{\varepsilon_{cc}}{\varepsilon_{co}} = 2 + 11.72\left(\frac{f_{lf}}{f_{co}}\right)^{0.55} + 5.8\left(\frac{f_{ls} + f_{lh}}{f_{co}}\right) \tag{7}$$

Referring to the confining mechanism of FRP confined CFST elements proposed by Hu (2011), in this study, the relationship between hoop strain (ε_h) and axial strain of confined concrete is calculated as:

$$\frac{\varepsilon_{cc}}{\varepsilon_{co}} + 0.66\left(1 + 8\frac{f_l}{f_{co}}\right) \times \left\{\left[1 + 0.75\left(\frac{\varepsilon_h}{\varepsilon_{co}}\right)\right]^{0.7} - \exp\left[-7\left(\frac{\varepsilon_h}{\varepsilon_{co}}\right)\right]\right\} = 0 \tag{8}$$

In the equations, f_{cc} is the compressive stress of confined concrete; f_{ls}, f_{lf} and f_{lh} are the confining stresses of steel tube, FRP and stirrups, respectively; f_l is the total confining pressure; E_c is the elastic modulus of concrete, which is taken as $4736 f_{co}^{0.5}$; ε_{cc} is the axial strain of confined concrete at its strength; σ_c is the axial stress of tested concrete specimen; ε_{co} is the axial strain of concrete at its strength; ε_c is the unit strain of concrete corresponding to σ_c.

As an analysis-oriented stress-strain model, the generation of the axial stress-strain curves for FRP-steel confined concrete would be achieved by an incremental process, which was introduced detailed in literature studied by the research group of the first author of the paper (Huang 2016).

b. Multi-cycle model

The cyclic constitutive model includes mainly the skeleton model and hysteretic law. The latter has two key unloading and reloading paths, and the calculation of plastic strain and stress degradation.

Here, the monotonic model proposed above is used to simulate the skeleton curve of the FRP-steel confined RC columns under cyclic loading. For the hysteretic models, considering the fact that the strength ratio of the FRP materials to steel is fairly large, the confining effectiveness of FRP-steel tube to the concrete is considered similar to that of the FRP-confined concrete. Meanwhile, due to the existence of the steel tube and transverse rebars in the FRP-steel confined RC columns, the authors suggest to use an improved model proposed by Lam and Teng (2009). The key features and related equations are presented in Fig. 14. The details of the multi-cyclic model are reached in the reference (Huang 2016).

5.1.3 A new material constitutive model for FRP-steel confined concrete developed with an OpenSees Programming

An accurate material constitutive model is the base of the analysis of the RC columns subjected to reversed cyclic loads. OpenSees is a well-known open source platform with a strong nonlinear structural analysis and a high compatibility. FRP-steel confined concrete can significantly improve the seismic behavior of the RC columns as demonstrated in Section 4 of the paper. However, the existing material constitutive models for FRP-steel confined concrete are not available in the current version of OpenSees. By the C++ programming language, a new user-defined material constitutive model based on the monotonic and multi-cycle constitutive model proposed in Section 5.1.2 was developed, and applied into an OpenSees platform. The developed new material constitutive model is suitable for FRP-steel confined concrete in circular section. The material models and elements are separate and independent in OpenSees. Therefore, all existing elements in OpenSees can be compatible with the new material model. Compared with the existing concrete model, the new developed material model can accurately simulate the true stress-strain relationship of FRP-steel confined concrete, especially the unloading rules including residual strain, which would improve the pinching effect of FRP-steel confined RC columns.

5.1.4 Steel model

In this study, a constitutive model of steel reinforcement proposed by Menegotto and Pinto (1973) was used considering steel reinforcement as an elastic-perfectly-plastic material, which is given as:

$$\sigma^* = b\varepsilon^* + \frac{(1-b)\varepsilon^*}{\left(1+\varepsilon^{*R}\right)^{1/R}} \tag{9}$$

where, b is strain hardening coefficient; σ* and ε* are normalized stress and strain. R is a curvature parameter. The detailed calculations of the parameters are available in the references (Menegotto and Pinto 1973, Orakcal et al.2006). Fig. 15 depicts a typical hysteretic stress–strain response output for steel reinforcement.

5.1.5 Cross-section rule

A distributed-plasticity, force-based nonlinear beam-column element was selected for the analysis of all columns. For FRP-steel confined RC columns, two beam-column elements were used to simulate the FRP confined hinge zone of 500 mm height and the remaining part of the column, respectively, which was described in Section 2.1. Similarly, two beam-column elements with the same element size were used for RC columns or steel tube confined RC columns. A cantilever half-column model was used in this simulation, which was used to be tested in this paper. As described in Section 2.1, the steel tubes and the FRP wrapping were terminated at their two ends to avoid the direct axial compression. Therefore, the steel tube and the FRP wrapping in the confined RC columns mainly provide the confining effect for the concrete core. In order to simply the simulation, the models of the stirrup, the steel tube and the FRP wrapping in the confined RC columns were not built in this paper, while the confining effects of the three parts on the concrete core were considered by introducing the above proposed stress-strain relationship of FRP-steel confined RC into the element, as demonstrated by Fig. 16. The circular cross-section of all columns was divided into 36 parts in hoop direction and 30 parts in radial direction. Therefore, 1080 fibers were used in the paper. The 1080 fibers (36*30 fibers) were determined according to the balance between computational accuracy and computational efficiency before ensuring convergence. However, a convergence study regarding the element size and fiber number was not conducted in this paper.

5.2 FEM model validation

Fig. 17 presents a comparison between the simulated and tested results of RC column and FRP-steel confined RC columns. It can be seen that the peak load of the simulated curves are very similar to their measured values, and the corresponding lateral displacements were also consistent with the test results. For the FRP-steel confined RC columns, the simulated curves were in good agreement with their experimental curves. Although a new material constitutive model for FRP-steel confined concrete, which would improve the pinching effect of the columns, was implemented in the analysis, the pinching effect of the simulated curves is still more obvious than that of the test curves, especially for the specimens G5S1T0, G7S1T0 and C7S1T0. This may be due to the fact that the slippage of steel rebar and concrete is not considered, which was neglected to simplify the simulation in this paper. Overall, the simulation results were in good agreement with the experimental results. Therefore, it is feasible to use the OpenSees-based FEM model to simulate the seismic performance of FRP-steel confined RC columns.

5.3 Parametric study of FRP-steel confined RC columns

To proper the seismic design of FRP-steel confined RC columns, it is necessary to understand the influence of main parameters on the seismic performance of the columns to make reliable adjustments accordingly based on laboratorial study. In this study, a parametric study was carried out on the effects of various parameters on the seismic preformation of FRP-Steel confined RC columns. The basic models from the above simulation program were used. The main structural parameters studied were axial load ratio (0.1-0.8), shear span ratio (2-10), steel tube thickness (1-6 mm), longitudinal steel ratio (change steel diameter), the number of FRP layers (1-8 layers), and the wrapping height of FRP sheet in the columns (0-1000 mm).

5.3.1 Effect of axial load ratio

Based on the tested specimens G0S1T0 and G5S1T0, the axial load ratio ranges from 0.1 to 0.8, as shown in Fig. 18, and the results demonstrate that during the increase of axial load, the bearing capacity

554 of the specimens decreased with an increased axial load more rapidly in post-peak. This shows that
555 the ductility got lower as the axial load ratio increased. The specimen G5S1T0 confined by 5-layer
556 GFRP sheet showed a better ductility than that of the specimen G0S1T0 confined only by steel tube.

557 ***5.3.2 Effect of shear span ratio***

558 Fig. 19 demonstrates the impact of shear span ratio on the seismic behaviour of the specimens
559 G0S1T0 and G5S1T0 without changing the other conditions. Results show that the effect of the shear
560 span ratio is basically the same when different types of external lateral confinement are used. As the
561 shear span ratios increased, the bearing capacity of the specimens decreased in turn. The peak
562 displacement also increased when shear span ratio increased meaning that the flexural capacity of the
563 columns was stronger.

564 ***5.3.3 Effect of the thickness of steel tube***

565 Fig. 20 shows the results when the thickness of steel tube increased from 1 mm to 6 mm in the
566 specimens G0S1T0 and G5S1T0, respectively. It is observed that as the thickness of steel tube
567 increased, the ductility and load carrying capacities of the specimens were improved. Moreover,
568 changing the thickness of steel tube has a greater influence on the specimen G0S1T0, as its bearing
569 capacity and ductility have been improved more significantly, and its peak strain became higher. On
570 the other hand, due to the lateral confinement of five layers of GFRP sheet was considered over-
571 confining, the effect of the thickness of steel tube on the specimen G5S1T0 was not very significant.
572 It is observed that when using FRP-steel tube to confine RC columns in practice, it is not advisable
573 to increase the thickness of steel tube in order to get a stronger confinement. It should be considered
574 that the simply increasing of the tube thickness would increase the self-weight of the structures, which
575 is not ideal for resisting the seismic actions.

576 ***5.3.4 Effect of longitudinal steel ratio***

577 The effect of longitudinal steel ratio on the seismic behaviour of FRP-steel confined RC columns was
578 examined by increasing the diameter of longitudinal reinforcement (D) of reference specimens. As

shown in Fig. 21, the results show that the bearing capacity of the two specimens is improved when the reinforcement ratio of longitudinal reinforcement increases, but the influence on the degradation ratio of the lateral load of the columns in post-peak is not obvious.

5.3.5 Effect of the layer number and confining height of FRP sheet

The effect of the number of FRP layers on the load-displacement skeleton curve of the columns is shown in Fig. 22. It was obtained that the lateral ultimate load and its corresponding displacement of the column increased as the number of GFRP layers increased. This indicates that as the number of GFRP layers increases, the bearing capacity and ductility of the columns is increased. On the other hand, based on the results of the specimen G5S1T0, the increase of the confining height of GFRP sheet (0, 300, 500, 800, and 1000 mm, respectively) has no significant effect on the bearing capacity and ductility of the specimens after the height reaches 300 mm. The height exceeds over 1.5 times of the diameter of the columns which is similar to the case in RC elements reported before. Therefore, the confining height of circular FRP-steel confined RC columns is suggested as 1.5 times of the column's diameter, which can make the columns achieve an economical and reasonable lateral confinement.

6. Discussions

6.1 Plastic Hinge Region (PHR) height

The predication of the lateral load–deformation behaviour of a concrete column involves an important step, modelling the plastic hinge region (PHR) of the column (e.g. Inel and Ozmen 2006, Youssf et al. 2015, Yuan *et al.* 2017). The region is defined as the deformation and damage region of elements, which experience inelastic demands. Based on the literature, previous experimental studies on concrete columns (unconfined or confined) assessed the PHR height by observing visually the damage regions at both ends of the columns (e.g. Bae and Bayrak 2008, Liu and Sheikh 2013). The damages mainly include cracks and spalling of concrete cover, which usually was considered that it relates to the longitudinal plastic deformations of the columns. For FRP confined concrete elements,

Ozbakkaloglu and Sattcioglu (2006, 2007) recommended using the hoop-strain profiles of the tubes to assess the PHR height, considering an intimate relationship between the lateral expansion of FRP tube and inside damage sustained by concrete. This means that the concrete cover may damage with a high probability when the corresponding hoop strain of FRP tube is high at the same position. Ozbakkaloglu and Idris (2014) suggested the PHR height can be established through a hoop-distribution of the specimens at its final loading cycle. They assumed that the PHR terminated at a height where the hoop strain fell below 1/3rd of the maximum-recorded strain in the cycle.

In this study, the PHR formation and propagation of the three types of tested columns, i.e. RC, confined RC and confined SRC columns, were determined based on a combined method considering the hoop strain evolution of the FRP-steel tube and the inside cracking formation of the specimens. The average PHR height of RC column in the current paper was obtained from the measured height of two sides of the column after the final load cycle. Regarding other confined RC/SRC columns, the PHR height of steel tube confined RC/SRC columns (G0S1T0 and G0S1T1) was determined by analysing the hoop-strain distribution of steel tubes along their height. For the FRP-steel confined RC/SRC columns, the experimental observation, and strain analyses were conducted to assess their PHR heights. The results presented in Figs. 5 and 7 show that the difference between the unconfined and confined columns is high which can be mainly attributed to the different lateral confinement conditions of the columns. The lateral confinement increases the ductility and deformability of the columns meaning their PHR heights reduce. In addition, the strain evolutions of the steel tube confined specimens and FRP-steel confined specimen such as G7S1T0 also show the difference of the deformation capacity of the region is between 70 mm and 220 mm from the end of the columns. The additional confinement from the FRP material increases the deformability of the confined RC/SRC columns. The PHR height of the specimen G7S1T0 should be between 70 mm to 220 mm, but it is more near to 70 mm. The damage shown in Fig. 5 verifies that the PHR height of the column G7S1T0 is about 100 mm. Comparing with the specimens G7S1T0 and C7S1T0, the higher elastic modulus and tensile strength of CFRP increases the hoop strain level at 220 mm from the end of the columns. However, the hoop strains of the CFRP-steel tube at 70 mm and 220 mm both are quite

631 small, which means its PHR height was not changed significantly being equal to that of GFRP-steel
632 confined RC columns. It can also be explained by the fact that CFRP and GFRP both are very strong
633 in tension compared with the steel tube. Within the SRC columns, there was no obvious difference
634 between the PHR height of steel tube confined SRC columns and FRP-steel confined SRC columns,
635 which both were about between 70 mm to 100 mm. As described previously, the H-section steel
636 already makes the RC columns be strong for the resistance of seismic action. This indicates that the
637 additional lateral confinement of FRP materials does not affect the deformability and ductility of the
638 columns.

639 **6.2 Peak drift level of confined RC columns**

640 As described previously, comparing with conventional RC columns, all confined RC columns of this
641 study presented an excellent seismic behaviour. However, the lateral load of the columns also started
642 to cause a degradation with an increase of the lateral displacement after reaching their peak load.
643 There were many researchers who had explained the reasons of the degradation (e.g. Ang 1985, Cai
644 *et al.* 2015) and indicated the degradation of RC columns with increasing lateral displacement was
645 very important considering safety aspects of the structures subjected to strong earthquake. To promote
646 the performance- or drift-based design of RC structures subjected to strong earthquake attacks, Cai *et*
647 *al.* (2015) proposed a complete shear design model for circular concrete columns, which was able to
648 predict the degradation of the lateral shear resistance of the columns under a mega-earthquake. As
649 shown in their model, Cai *et al.* (2015) pointed out that the effective lateral confinement factor (I_c) of
650 circular RC columns had a significant influence on the peak drift ratio of the columns, which was
651 denominated as the degradation-starting drift ratio R_{iu}. The drift ratio is calculated by a ratio of Δ_{max}/L
652 (where, Δ_{max} is the displacement corresponding to peak load point and L is the shear span of the
653 columns). For discussing the drift ratio of the confined RC columns, this study collected several RC
654 columns confined by steel tube or FRP-steel tube by existing literature (Liu *et al.* 2009, Zhou and Liu
655 2010, Gan *et al.* 2011, Lin 2012). Using the FEM analysis results in this paper, a data set of the
656 confined RC columns with shear span ratio (a/D) larger than 1.5 and axial load ratio (n) exceeding of

0.3 was modelled and analysed. In theory, these columns have a stronger trend to fail as flexural failure mode. Referring to the model developed by Cai et al. (2015), the effective lateral confinement factor (I_c) of FRP-steel confined RC columns is calculated by

$$I_c = \frac{\rho_{hs} \cdot f_{hs}}{f_{co}} + \frac{\rho_{hst} \cdot f_{hst}}{f_{co}} + \frac{\rho_{hfrp} \cdot f_{hfrp}}{f_{co}} \quad (10)$$

where $\rho_{hs}$is the volume ratio of stirrup; ρ_{hst} and ρ_{hfrp} is the equivalent stirrup volume ratio of the steel tube and the FRP tube, respectively; f_{hs} and f_{hst} are the yield strength of the stirrup and the steel tube, respectively; f_{hfrp} is the hoop stress of the FRP tube at peak point taken as about 10% of ultimate strength of FRP according to the test results;

Fig.23 shows the relationship between peak drift ratio R_{iu} and the effective lateral confinement factor I_c of the columns confined by the steel or FRP-steel tube, by steel tube and by FRP-steel tube. Results show that the factor I_c has a different influence on the peak drift level of circular confined RC columns comparing with the case in circular RC columns. According to existing design codes, most of circular RC columns have an I_c factor less than 0.3 and have a peak drift varying from 0.5% to 2.5%. The increasing of I_c brings a larger increase in the peak drift ratio in Cai *et al.* model (Cai et al. 2015). This can be explained by the fact that the increase of lateral confinement of RC columns has a more significant effect on the enhancement of peak drift ratio of shear-dominant columns. In the data established in the paper, however, all confined columns are flexural-dominant columns. Besides, the I_c factors of the RC columns confined by steel or FRP-steel tube had a larger varying region. The peak drifts ratios of the columns increased with the I_c factors. Comparing with the case of steel tube or FRP-steel tube confined RC columns, a stronger linear relationship was found between the I_c factor and the peak drift ratio R_{iu} of steel tube confined RC columns. However, as shown in Fig.23, the existing data of FRP-steel tube confined columns is not enough for determining the relationship between I_c and R_{iu} in these columns. Therefore, the paper suggests that peak drift ratio R_{iu} of the RC columns confined by steel tube or FRP-steel tube can be calculated simply at the beginning by

$$R_{iu} = 2.6I_c + 0.8 \quad \text{(in \%)} \quad (11)$$

7. Concluding Remarks

This paper investigated the behaviour of FRP-steel confined concrete columns under reversed cyclic lateral loads through a series of experiments, including RC (reference column), steel tube confined RC/SRC columns, and FRP-steel confined RC/SRC columns. Flexural failures were observed for all columns. The following conclusions can be made:

- With the increase of the number of FRP layers, the structural behaviours (including yield load and displacement, peak load and displacement, ultimate load and displacement, and ductility coefficient) of the FRP-steel confined RC/SRC columns have been improved.
- The load-carrying capacity, ductility and energy dissipation capacity of FRP-steel confined RC columns were better than those of RC columns and steel tubes confined RC columns. Moreover, the improvement caused by the lateral confinement increased as the number of layers of FRP increased. Similar observations occurred in FRP-steel confined SRC columns when comparing with SRC column or steel tube confined SRC column.
- FRP wrapping has no significant effect on the initial stiffness of FRP-steel confined RC/SRC columns. However, with the increase of the lateral displacement and with more layers of FRP sheet confining, the stiffness degradation of the columns was reduced.

Based on the proposed FEM model verified by the test results in the paper, a parametric analysis has been conducted to analyse main factors on the behaviour of GFRP-steel confined RC columns. The main observations are as follows:

- With the increase of the axial load ratio and the shear span ratio, the load-bearing capacity of steel tube confined and FRP-steel confined RC columns has been improved, while the ductility of the columns has been significantly reduced.
- The load-bearing capacity of steel tube and FRP-steel confined RC columns increased as the thickness of steel tube increased, while the former kind of the columns increased more significantly. However, the thickness has no significant influence on the ductility of the columns.
- The increase of the longitudinal reinforcement ratio improved the load-bearing capacity of steel

tube and FRP-steel confined RC columns but just has little effect on the ductility of the columns.

- The increase of the number of FRP layers enhanced the ultimate load-bearing capacity and ductility of FRP-steel confined RC columns, but the positive effect was weakened after a certain number of FRP layers were applied. It is need more studies to quantify this for the FRP-steel confined RC columns. The change in the height of FRP wrapping has no significant influence on the load-bearing capacity and ductility the columns after the height reaches 1.5 times of the column's diameter.

On the other hand, this study discussed the influence of main variables on the plastic hinge region (PHR) height and peak drift ratio of the confined RC columns under reversed cyclic loads and presented that the lateral confinement condition has a significant influence on the PHR height and peak drift ratio of the confined RC columns. Based on the existing test data, the paper suggests a simple model to predict the peak drift ratio of the confined RC columns as well.

Acknowledgements

This work was supported by the National Key R&D Program of China (Project No. 2017YFC0703008), the National Natural Science Foundation of China (Project No.51778102, 51708433), the Fundamental Research Funds for the Central Universities (Project No. DUT18LK35)and the Natural Science Foundation of Liaoning Province of China (Project No. 20180550763).

References

Aboutaha, R. S., and Machado, R. I. (1999). "Seismic resistance of steel-tubed high-strength reinforced-concrete columns." *J. Struct. Eng.*, *125*(5), 485-494.

Ang, B.G. (1985). "Seismic shear strength of circular bridge piers." *Rep. No. 85-5,* Department of Civil Engineering, University of Canterbury, Christchurch, New Zealand.

Bae, S., and Bayrak, O. (2008). "Plastic hinge length of reinforced concrete columns." *ACI Struct. J.*, *105*(3), 290.

734 Binici, B. (2005). “An analytical model for stress–strain behavior of confined concrete.” *Eng.*
735 *Struct.*, *27*(7), 1040-1051.
736 Cai, G., Sun, Y., Takeuchi, T., and Zhang, J. (2015). “Proposal of a complete seismic shear strength
737 model for circular concrete columns.” *Eng. Struct.*, *100*, 399-409.
738 Cao, Q., Tao, J., Wu, Z., and Ma, Z. J. (2017). “Behavior of FRP-Steel Confined Concrete Tubular
739 Columns Made of Expansive Self-Consolidating Concrete under Axial Compression.” *J. Compos.*
740 *Constr.*, *21*(5), 04017037.
741 Gan, D., Guo, L., Liu, J., and Zhou, X. (2011). “Seismic behavior and moment strength of tubed
742 steel reinforced-concrete (SRC) beam-columns.” *J. Constr. Steel Res.*, *67*(10), 1516-1524.
743 GB 50010-2010. (2015). “Code for design of concrete structures.” Ministry of House and Urban-
744 Rural Development of People’s Republic of China, Beijing (in Chinese)
745 GB/T228-2010. (2009). “Tensile test method for the metal materials at room temperature.”
746 Standardization Administration of the People’s Republic of China, Beijing 2010. (in Chinese)
747 Han, L. H., Liu, W., and Yang, Y. F. (2008). “Behavior of thin walled steel tube confined concrete
748 stub columns subjected to axial local compression.” *Thin Wall Struct.*, *46*(2), 155-164.
749 Han, L. H., Qu, H., Tao, Z., and Wang, Z. F. (2009). “Experimental behaviour of thin-walled steel
750 tube confined concrete column to RC beam joints under cyclic loading.” *Thin Wall Struct.*, *47*(8-9),
751 847-857.
752 Han, L. H., Yao, G. H., Chen, Z. B., and Yu, Q. (2005). “Experimental behaviours of steel tube
753 confined concrete (STCC) columns.” *Steel Compos. Struct.*, *5*(6), 459-484.
754 Hu, H. and Seracino, R. (2013). “Analytical model for FRP-and-steel-confined circular concrete
755 columns in compression.” *J. Compos. Constr.*, *18*(3), A4013012.
756 Hu, Y. M., Yu, T. and Teng, J. G. (2011). “FRP-Confined Circular Concrete-Filled Thin Steel
757 Tubes under Axial Compression.” *J. Compos. Constr.,* 15(5), 850-860.
758 Huang, P.D. (2016). "Cyclic Axial Compression Mechanical Behavior Study of GFRP-Steel
759 Composite Tube Confined RC Stub Columns." MS Thesis of Dalian University of Technology,

760 Dalian. [In Chinese]

761 Inel, M., and Ozmen, H. B. (2006). “Effects of plastic hinge properties in nonlinear analysis of

762 reinforced concrete buildings.” *Eng. Struct.*, *28*(11), 1494-1502.

763 JGJ3-2002. (2002). “Technical Specification for Concrete Structures of Tall Buildings.”

764 Standardization Administration of the People’s Republic of China, Beijing; 2002. (in Chinese)

765 Jiang, T., and Teng, J. G. (2007). “Analysis-oriented models for FRP-confined concrete.” *Eng.*

766 *Struct.*, *29*, 2968-2986.

767 Kent, D.C. and Park, R. (1971) “Flexural members with confined concrete.” *J. Struct. Division*,

768 97(7), 1969-1990.

769 Lam, L., and Teng, J.G. (2009). “Stress-strain model for FRP-confined concrete under cyclic axial

770 compression”. *Eng. Struct.*, 31(2), 308-321.

771 Li, Y. F., Chen, S. H., Chang, K. C., and Liu, K. Y. (2005). “A constitutive model of concrete

772 confined by steel reinforcements and steel jackets.” *Can. J. Civil Eng.*, *32*(1), 279-288.

773 Lin, S. L. (2012). “Seismic performance of FRP-steel composite tube confined RC columns.” *MS*

774 *Thesis of Harbin Institute of Technology*, Harbin. (In Chinese)

775 Liu, J. P., Xu, T. X., Wang, Y. H., and Guo, Y. (2018). “Axial behaviour of circular steel tubed concrete

776 stub columns confined by CFRP materials.” *Constr. Build Mater.*, *168*, 221-231.

777 Liu, J., and Sheikh, S. A. (2013). “Fiber-reinforced polymer-confined circular columns under

778 simulated seismic loads.” *ACI Struct. J.*, *110*(6), 941.

779 Liu, J., Zhang, S., Zhang, X., and Guo, L. (2009). “Behavior and strength of circular tube confined

780 reinforced-concrete (CTRC) columns.” *J. Constr. Steel Res.*, *65*(7), 1447-1458.

781 Liu, L., and Lu, Y. (2010). “Axial bearing capacity of short FRP confined concrete-filled steel

782 tubular columns.” *J. Wuhan Univ. Tech.-Mater. Sci. Ed.*, *25*(3), 454-458.

783 Mazzoni, S., McKenna, F., Scott, M.H., and Fenves, G.L. (2006). *OpenSees command language*

784 *manual.* Pacific Earthquake Engineering Research (PEER) Center.

785 Menegotto, M., and E. Pinto. (1973). “Method of analysis for cyclically loaded reinforced concrete
786 plane frames including changes in geometry and non-elastic behavior of elements under combined
787 normal force and bending.” *Proc., IABSE Symposium.* Lisbon, Portugal, 15-22.
788 Orakcal, K., Massone, L.M.,Wallence, J.W. (2006). “Analytical modeling of reinforced concrete
789 walls for predicting flexural and coupled-shear-flexural responses.” PEER, University of California.
790 USA.
791 Ozbakkaloglu, T., and Idris, Y. (2014). “Seismic behavior of FRP-high-strength concrete–steel
792 double-skin tubular columns.” *J. Struct. Eng.*, *140*(6), 04014019.
793 Ozbakkaloglu, T., and Saatcioglu, M. (2006). “Seismic behavior of high-strength concrete columns
794 confined by fiber-reinforced polymer tubes.” *J. Compos. Constr.*, *10*(6), 538-549.
795 Ozbakkaloglu, T., and Saatcioglu, M. (2007). “Seismic performance of square high-strength
796 concrete columns in FRP stay-in-place formwork.” *J. Struct. Eng.*, *133*(1), 44-56.
797 Park, J. W. and Choi, S. M. (2013). “Structural behavior of CFRP strengthened concrete-filled
798 steel tubes columns under axial compression loads”. *Steel Compos. Struct.*, 14(5), 453-472.
799 Park, J. W., Hong, Y. K. and Choi, S. M. (2010). “Behaviors of concrete filled square steel tubes
800 confined by carbon fiber sheets (CFS) under compression and cyclic loads.” *Steel Compos.*
801 *Struct.*, *10*(2), 187-205.
802 Park, R. (1988). “State of the art report ductility evaluation from laboratory and analytical testing.”
803 *Proc., 9th World Conf. Earthq. Eng.*, Tokyo, Kyoto, Japan, 605-616.
804 Popovics, S. (1973). “A numerical approach to the complete stress-strain curve of
805 concrete.” *Cement Concrete Res.*, *3*(5), 583-599.
806 Ran J.H. (2014). “Axial Compression Mechanical Behavior of FRP-Steel Composite Tube
807 Confined Concrete Stub Columns.” *MS Thesis of Dalian University of Technology*, Dalian. [In
808 Chinese]
809 Sakino, K., Nakahara, H., Morino, S., and Nishiyama, I. (2004). Behavior of centrally loaded
810 concrete-filled steel-tube short columns. *J. Struct. Eng.*, *130*(2), 180-188

811 Scott, B. D., Park, R., and Priestley, M. J. N. (1982). "Stress-strain behavior of concrete confined
812 by overlapping hoops at low and high strain rates." *ACI Struct. J.*, 79(1), 13-27.
813 Tao, Z., Wang, Z., Han, L. and Uy, B. (2011). "Fire performance of concrete-filled steel tubular
814 columns strengthened by CFRP." *Steel Compos. Struct.*, 11(4), 307-324.
815 Teng, J. G., Hu, Y. M. and Yu, T. (2013). "Stress–strain model for concrete in FRP-confined steel
816 tubular columns." *Eng. Struct.*, 49(2),156-167.
817 Tomii, M., Sakino, K., Watanabe, K. and Xiao, Y. (1985a). "Lateral load capacity of reinforced
818 concrete short columns confined by steel tube", *Proc., Int'l Speciality Conf. Concr. Filled Steel*
819 *Tubular Struct.*, Harbin, China, August, pp. 19-26.
820 Tomii, M., Sakino, K., Xiao, Y. and Watanabe, K. (1985b). "Earthquake resisting hysteretic
821 behavior of reinforced concrete short columns confined by steel tube", *Proc., Int'l Speciality Conf.*
822 *Concr. Filled Steel Tubular Struct.*, Harbin, China, August, pp. 119-125.
823 Wang, D.Y. (2012). "Experimental and analytical investigation of seismic performace of nonductile
824 RC frames retrofitted with FRP." *Ph.D Dissertation of Harbin Institute of Technology*, Harbin. (in
825 Chinese)
826 Wang, Z., Yu, Q. and Tao, Z. (2015). "Behaviour of CFRP externally-reinforced circular CFT
827 members under combined tension and bending." *J. Constr. Steel Res.*, 106, 122-137.
828 Wu, Z., Wang, X., Zhao, X., and Noori, M. (2014). "State-of-the-art review of FRP composites for
829 major construction with high performance and longevity." *J. Sustainable Mater. Struct. Sys.*, *1*(3),
830 201-231.
831 Xiao, Y. (2004). "Applications of FRP composites in concrete columns." *Adv. Struct. Eng.*, *7*(4),
832 335-343.
833 Xiao, Y., He, W., and Choi, K. K. (2005). "Confined concrete-filled tubular columns." *J. Struct.*
834 *Eng.*, *131*(3), 488-497.
835 Youssf, O., ElGawady, M. A., and Mills, J. E. (2015). "Displacement and plastic hinge length of
836 FRP-confined circular reinforced concrete columns." *Eng. Struct.*, *101*, 465-476.

837 Yu, Q., Tao, Z., Liu, W., and Chen, Z. B. (2010). “Analysis and calculations of steel tube confined
838 concrete (STCC) stub columns.” *J. Constr. Steel Res.*, *66*(1), 53-64.
839 Yu, T., Hu, Y. M. and Teng J. G. (2016). “Cyclic lateral response of FRP-confined circular
840 concrete-filled steel tubular columns.” *J. Constr. Steel Res.,* 124, 12-22.
841 Yuan, F., Wu, Y. F., and Li, C. Q. (2017). “Modelling plastic hinge of FRP-confined RC
842 columns.” *Eng. Struct.*, *131*, 651-668.
843 Zhou, X. H., Liu, J. P., Wang, X., and Chen, Y. F. (2016). “Behavior and design of slender circular
844 tubed-reinforced-concrete columns subjected to eccentric compression.” *Eng. Struct., 124*, 17-28.
845 Zhou, X. H., Yan, B., and Liu, J. P. (2015). “Behavior of square tubed steel reinforced-concrete
846 (SRC) columns under eccentric compression.” *Thin Wall Struct.*, *91*, 129-138.
847 Zhou, X., Cheng, G., Liu, J., Gan, D., and Chen, Y. F. (2017). “Behavior of circular tubed-RC
848 column to RC beam connections under axial compression.” *J. Constr. Steel Res.*, *130*, 96-108.
849 Zhou, X.H., and Liu, J. P. (2010). “Seismic behavior and shear strength of tubed RC short
850 columns.” *J. Constr. Steel Res.*, *66*(3), 385-397.

Tables

Table 1 Details of test specimens

Table 2 Material properties of steel, FRP and epoxy adhesive

Table 3 Summary of the test results of test specimens

Table 1 Details of test specimens

Test No.	Diameter D /mm	Thickness t_s /mm	Reinforcing bars	Stirrups	The number of layers of FRP sheet	FRP type	Setting of H-Steel
G0S0T0	300	-	6Φ16	Φ8@100	-	-	No
G0S1T0	300	3			-	-	No
G5S1T0	300	3			5	GFRP	No
G7S1T0	300	3			7	GFRP	No
C7S1T0	300	3			7	CFRP	No
G0S1T1	300	3			-	-	Yes
G5S1T1	300	3			5	GFRP	Yes
G7S1T1	300	3			7	GFRP	Yes

Noted: G/Cx: x-layers GFRP or CFRP sheet; S0/S1: without/with confined steel tube; T0/T1: without/with H-steel;

Table 2 Material properties of steel, FRP and epoxy adhesive

Materials	Diameter or thickness (mm)	Young's modulus E_s /GPa	Yielding strength f_y /MPa	Tensile strength f_u /MPa
Steel tube Q235	3	210	280	414
Stirrups Q345	8	206	400	540
Reinforcing rebar Q345	16	205	420	590
H-Steel wing/web plates	10/7	208/221	223/225	374/387
Materials	**Thickness t_{frp} /mm**	**Young's modulus E /GPa**	**Elongation δ /%**	**Tensile strength f /MPa**
CFRP	0.167	245	1.51	4077
GFRP	0.354	72	2.1	1500
Epoxy	-	≥2.4	≥1.50	≥38

Table 3 Summary of the test results of test specimens

Specimens	P_y	Δ_y/mm	P_{max}/kN	Δ_{max}/mm	P_u/kN	Δ_u/mm	R/%	μ_Δ
G0S0T0	80.55	8.30	92.95	13.42	79.01	16.44	1.37	1.98
G0S1T0	96.44	10.49	110.95	21.68	94.30	43.90	3.66	4.19
G5S1T0	101.84	12.37	122.29	24.91	103.95	52.11	4.34	4.21
G7S1T0	107.01	14.53	128.72	27.83	109.41	62.70	5.23	4.32
C7S1T0	103.81	11.52	122.97	24.60	104.53	51.37	4.28	4.46
G0S1T1	149.83	13.99	158.45	35.79	134.68	72.64	6.05	5.19
G5S1T1	150.34	14.78	172.46	36.22	155.22	77.81	6.48	5.26
G7S1T1	165.07	15.47	186.78	39.75	168.10	81.99	6.83	5.30

Noted: μ_Δ is displacement ductility coefficient, which is calculated by Δ_u/Δ_y.

Fig.1

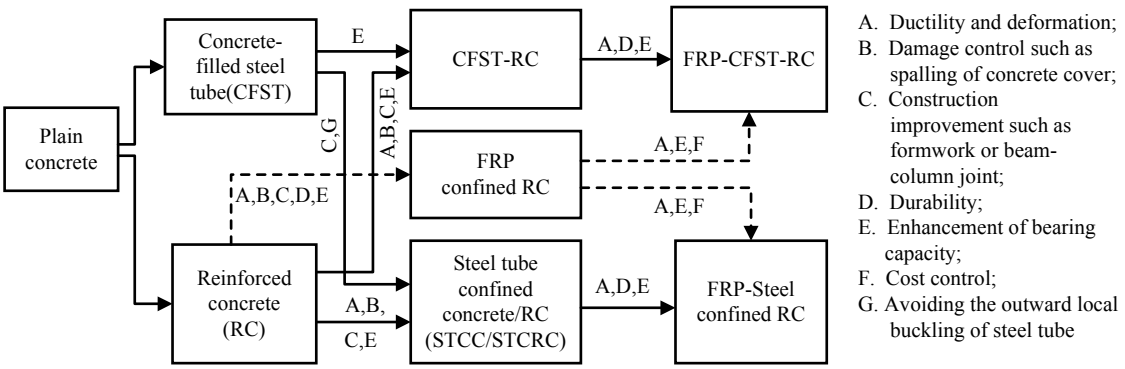

Fig.1 Development of reinforced concrete and confined concrete in past decades

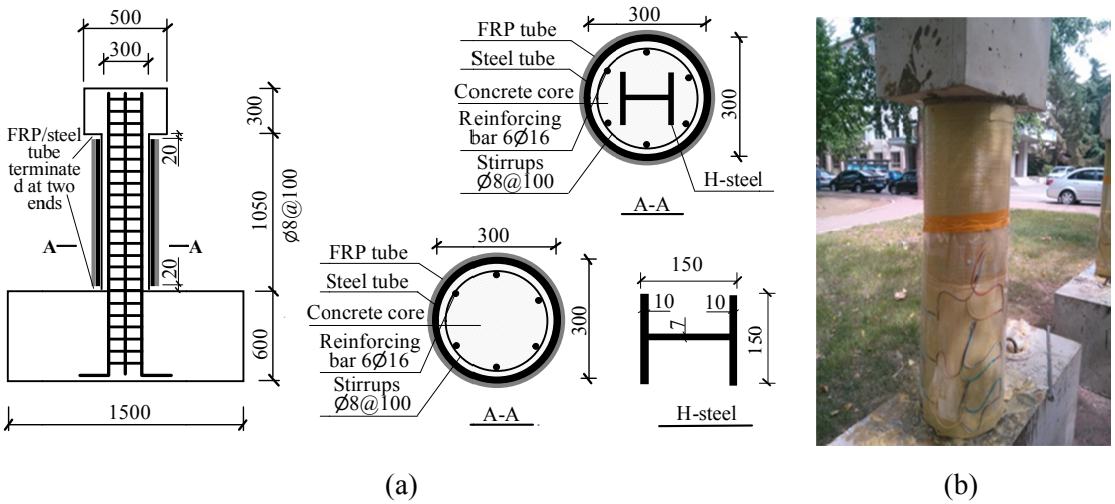

(a) (b)

Fig. 2 Details of test specimens (Units in mm): (a) Dimension and reinforcement arrangement; (b) Confined columns

Fig.3

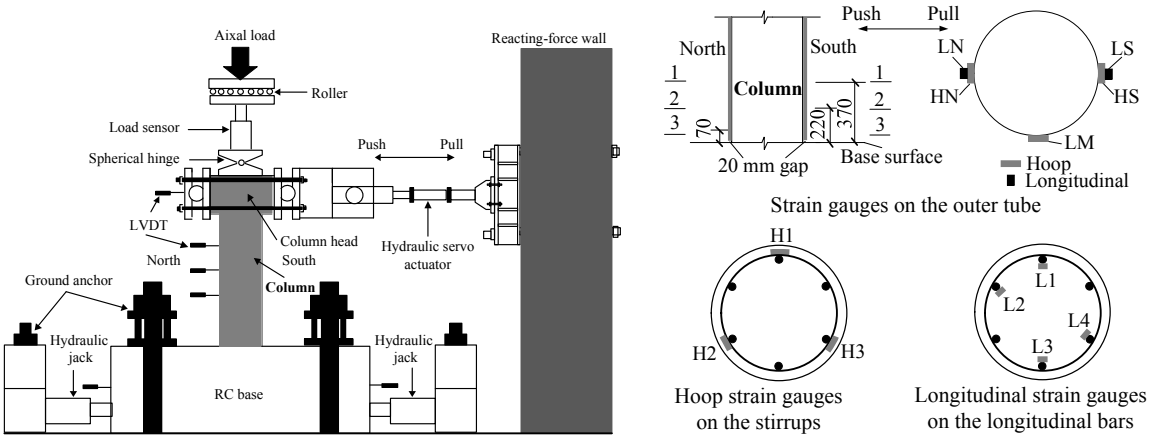

Fig. 3 Test setup and layout of LVDTs and strain gauge (Units in mm)

Fig.4

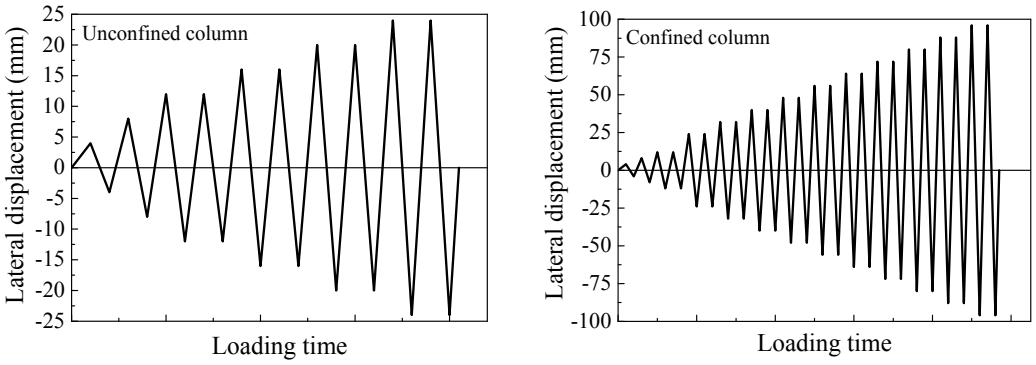

Fig. 4 Loading procedure

Fig.5

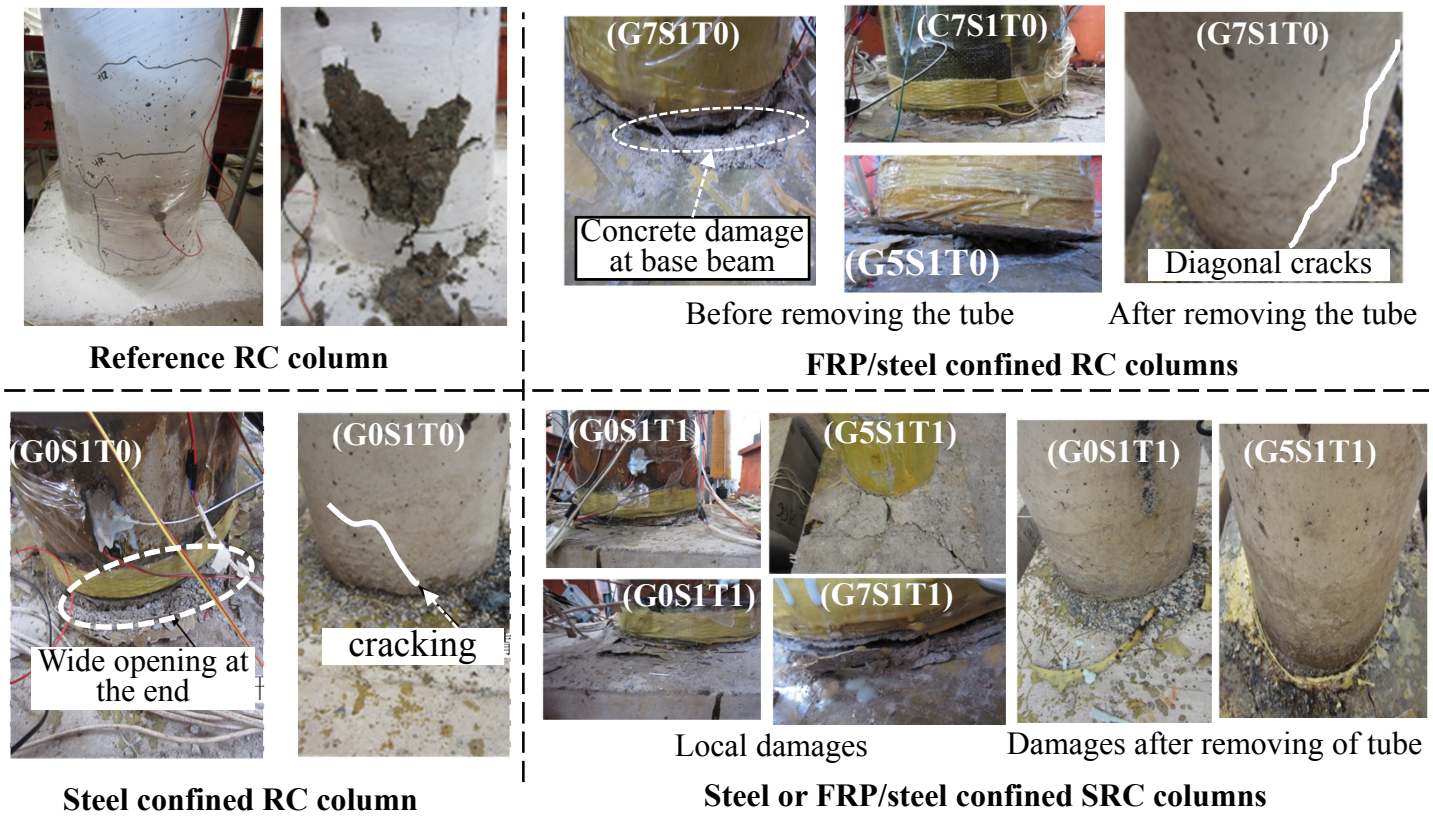

Fig. 5 Damages and cracks of the specimens

Fig.6

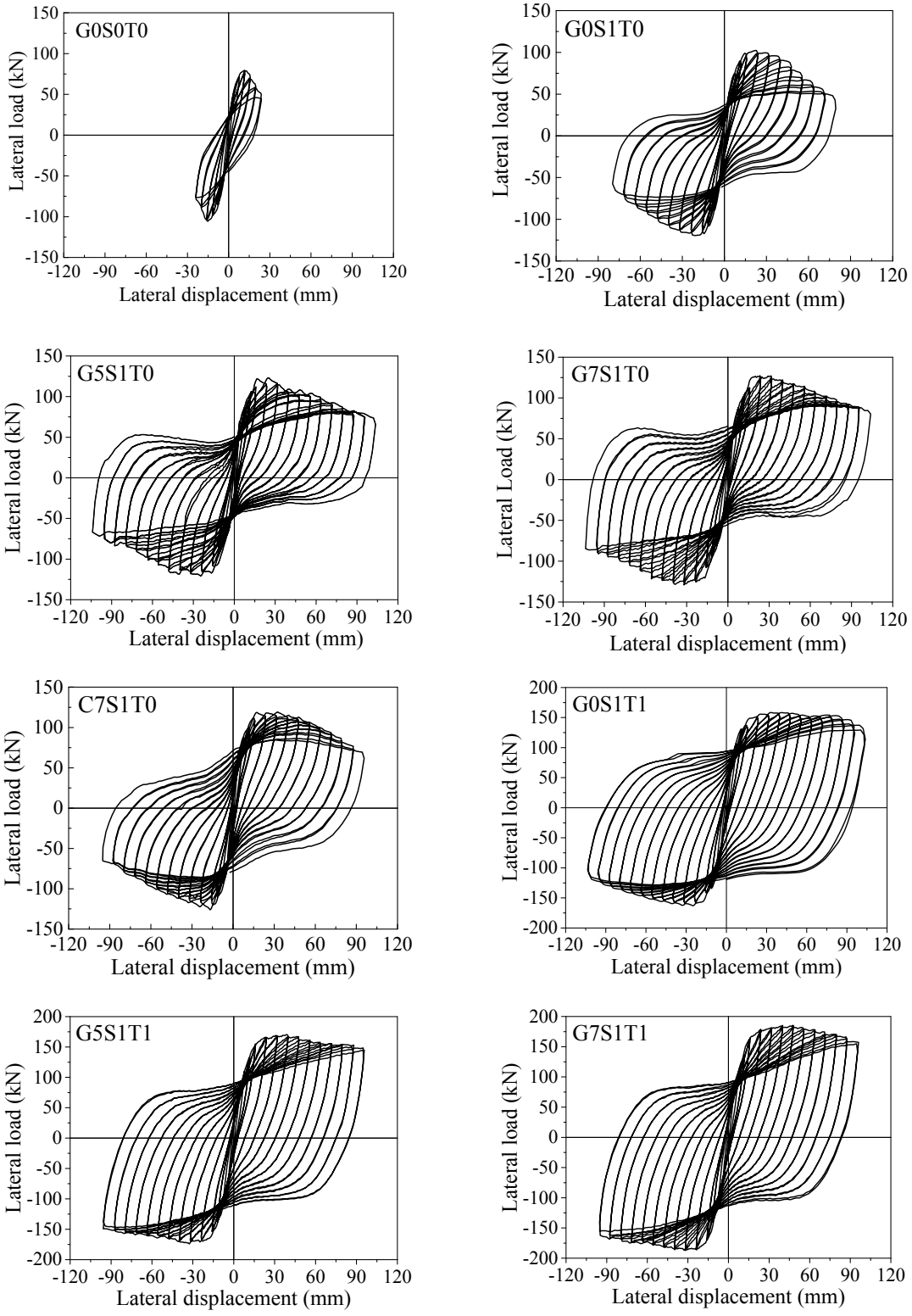

Fig.6 Hysteresis behavior of the specimens

Fig.7

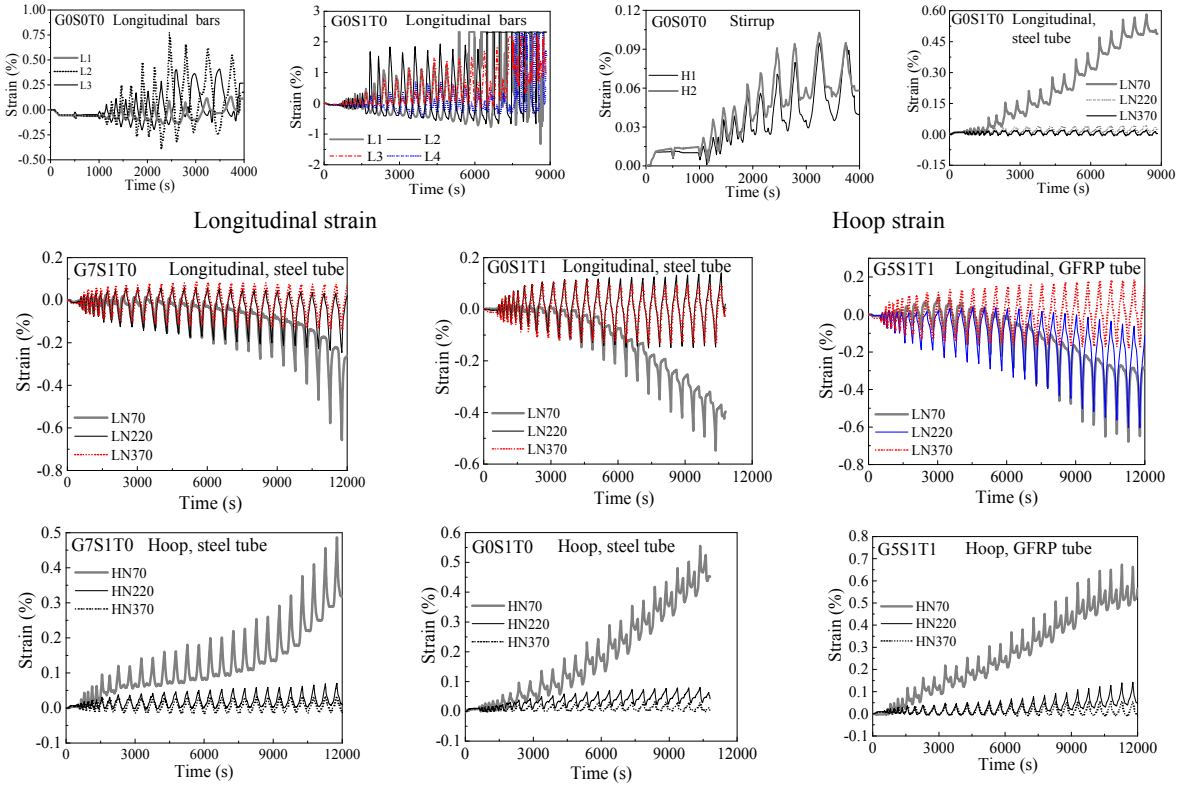

Fig. 7 Strain evolution of reinforcing bars, steel tube and FRP tube

Fig.8

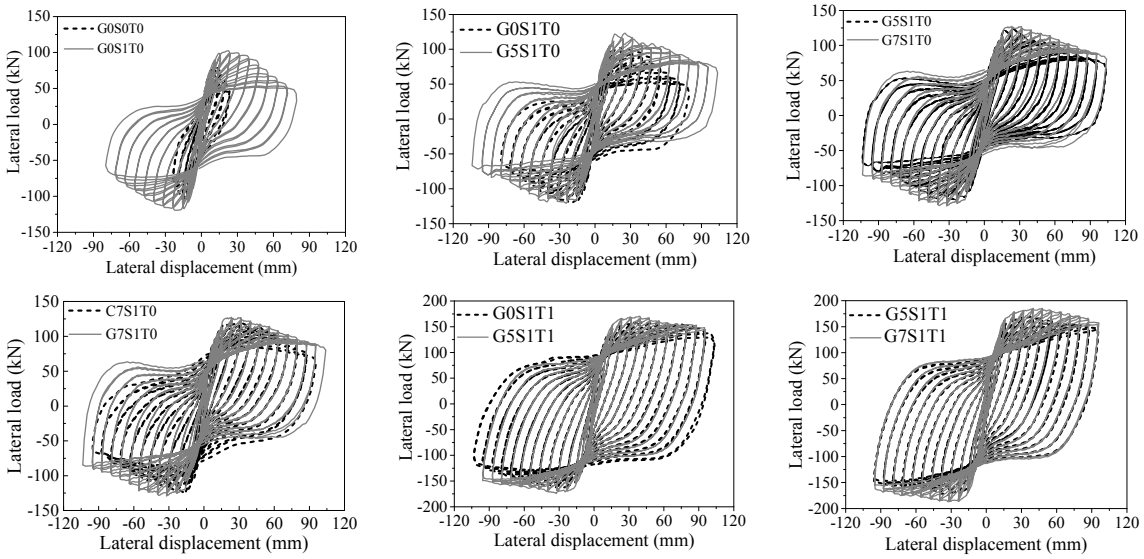

Fig. 8 Comparison of experimental lateral load-displacement curves

Fig.9

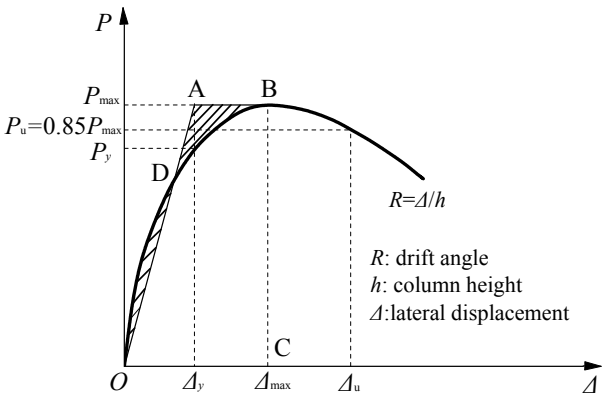

Fig. 9 Ductility calculation method – the equivalent elastoplastic energy absorption method (Park 1988)

Fig.10

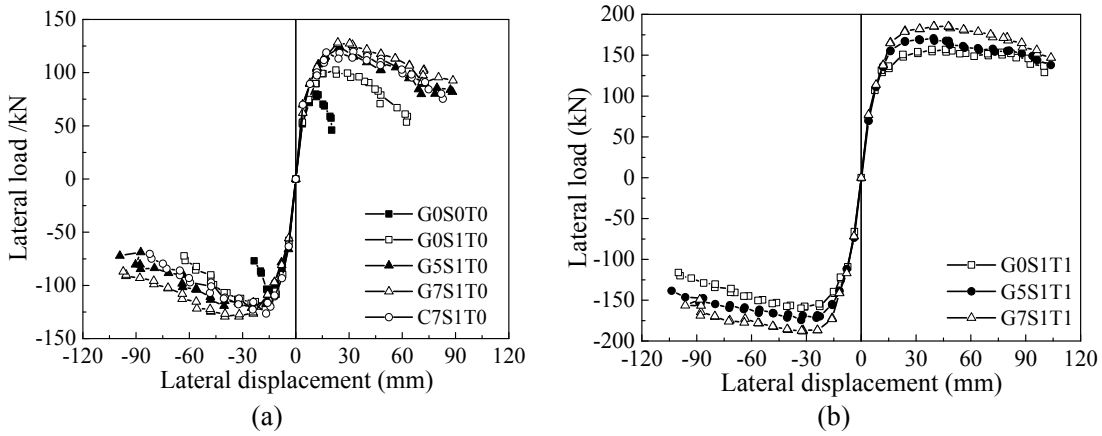

Fig. 10 Experimental load-displacement skeleton curves: (a) Without H-steel; (b) With H-steel

Fig.11

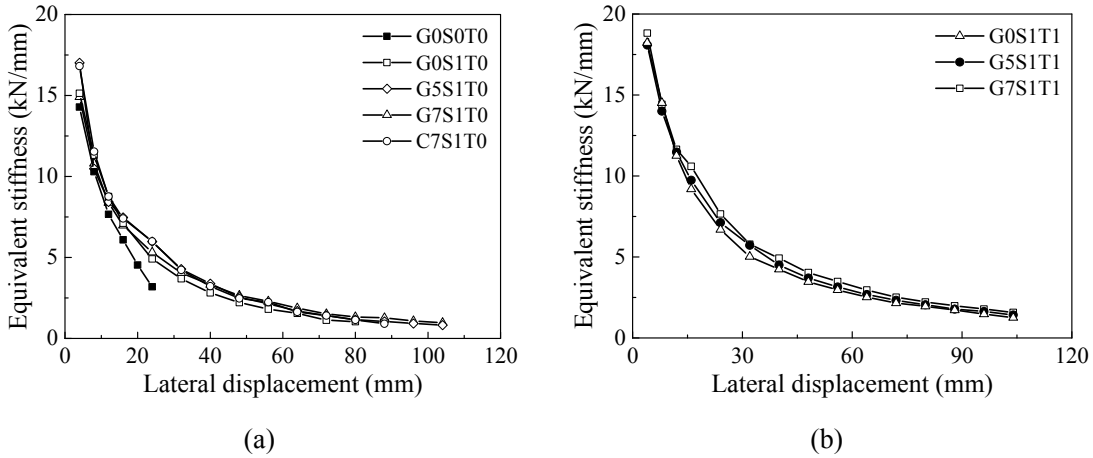

Fig. 11 Evolution of the equivalent stiffness of test specimens: (a) Without H-steel; (b) With H-steel

Fig.12

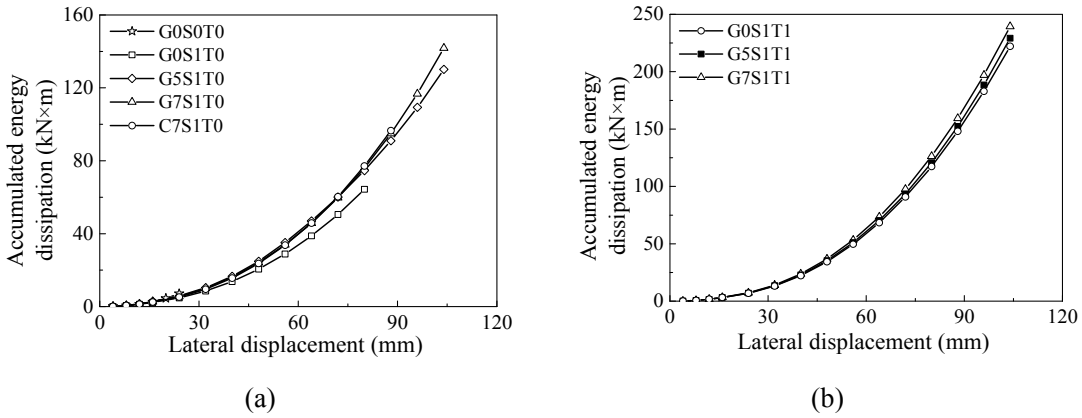

(a) (b)

Fig. 12 Accumulated energy dissipation of the test specimens: (a) Without H-steel; (b) With H-steel

Fig.13

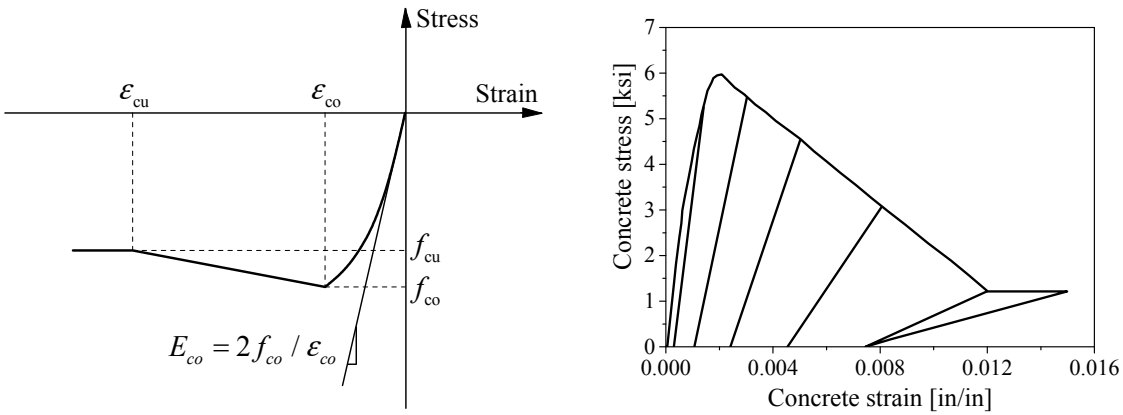

Fig. 13 Stress-strain models of Concrete01 in OpenSees (Mazzoni et al. 2006)

Fig.14

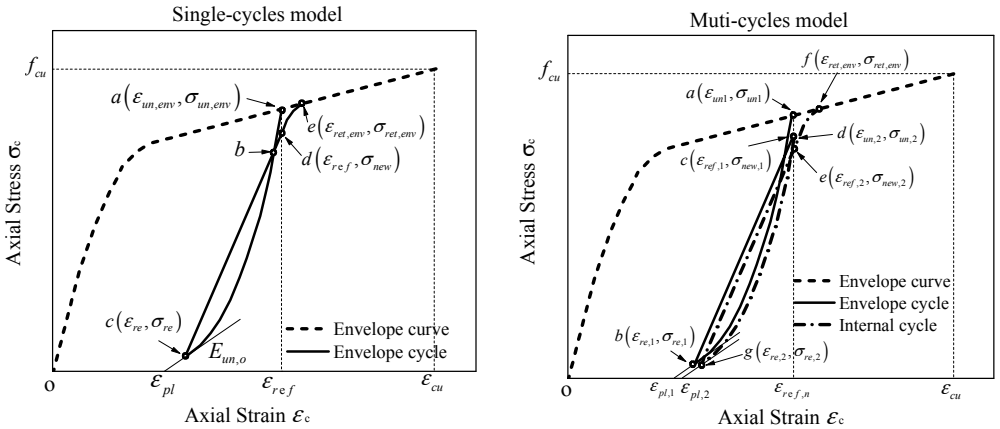

$$\varepsilon_{pl,n}=\begin{cases}0 & 0.0<\varepsilon_{un,env}\le 0.001 & n=1\\ k_5[1.4(0.87-0.004f_{co}^{'})-0.64]\left(\varepsilon_{un,env}-0.001\right) & 0.001<\varepsilon_{un,env}\le 0.0035 & n=1\\ \left(0.87-0.004f_{co}^{'}\right)\varepsilon_{un,env}-k_6 & 0.0035<\varepsilon_{un,env}\le\varepsilon_{cu} & n=1\\ \left(1-\omega_n\right)\varepsilon_{un,n}+\omega_n\varepsilon_{pl,n-1} & & n\ge 2\end{cases}$$

$$\gamma_{re,n}=\frac{\varepsilon_{un,n+1}-\varepsilon_{pl,n}}{\varepsilon_{ref,n}-\varepsilon_{pl,n}} \qquad \sigma_{new,n}=\varphi_n\sigma_{ref,n}$$

$$\sigma_c=a\varepsilon_{x,c}^{\eta}+b\varepsilon_{x,c}+c \qquad \eta=350\varepsilon_{un}+3$$

Fig. 14 Key parameters of proposed cyclic constitutive models (Huang 2016)

Fig.15

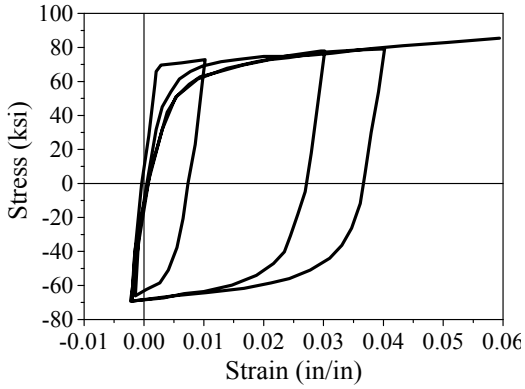

Fig. 15 Hysteretic property of Steel02 model in OpenSees

Fig.16

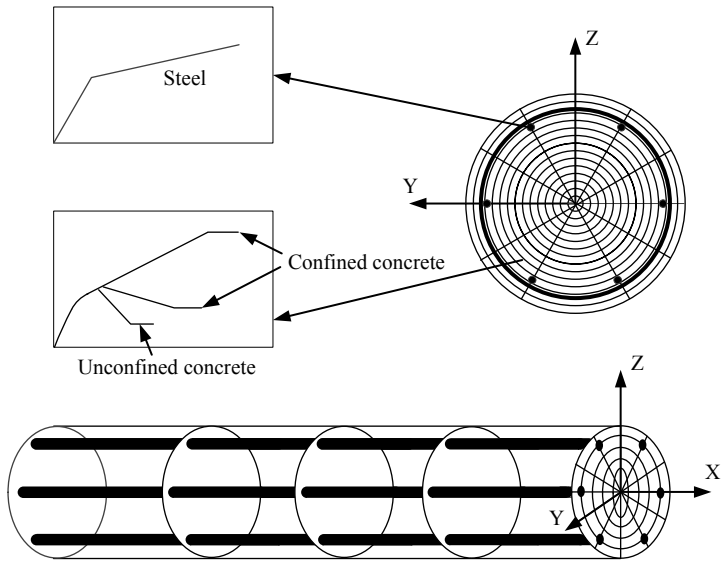

Fig. 16 Schematic representation of the fibre's cross-section

Fig.17

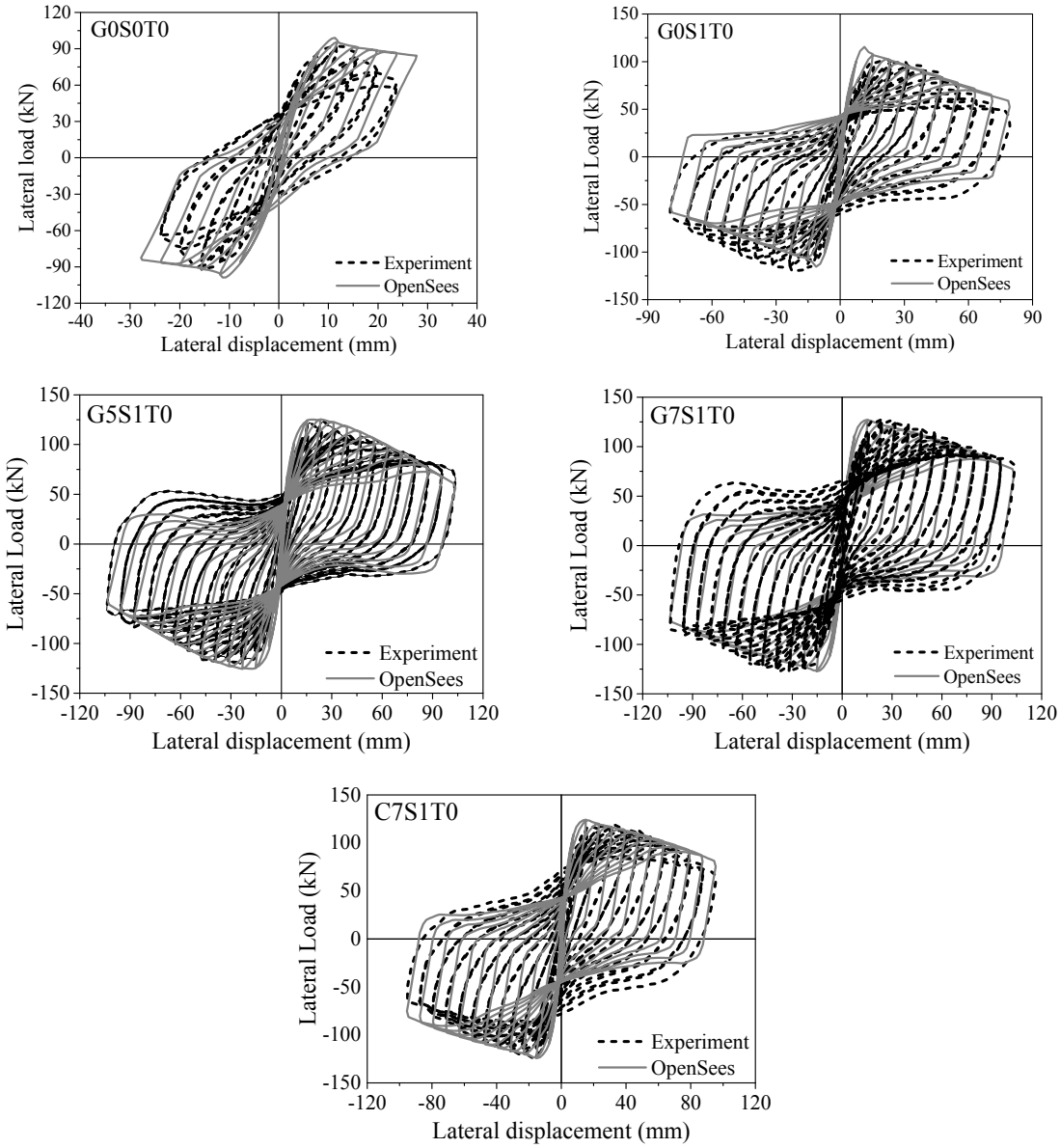

Fig. 17 Comparison between simulation and test results of circular RC and confined RC columns

Fig.18

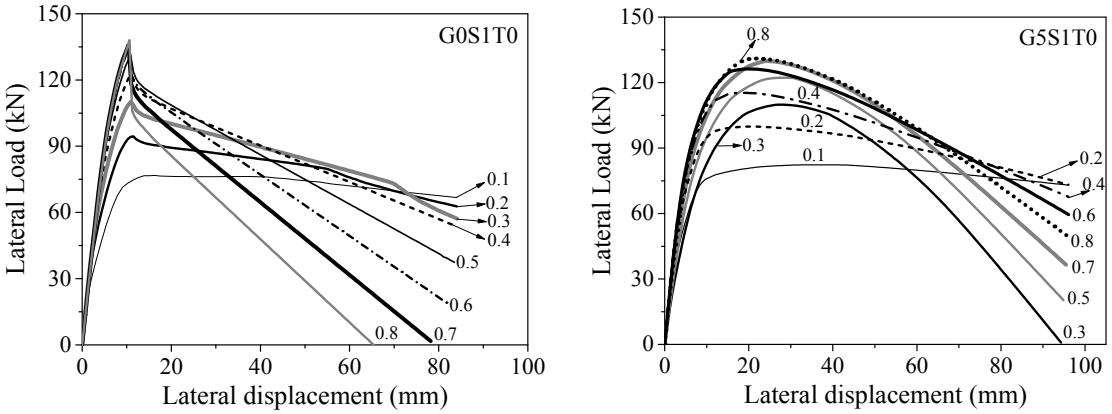

Fig. 18 Influence of axial load ratio on FRP-steel confined RC columns

Fig.19

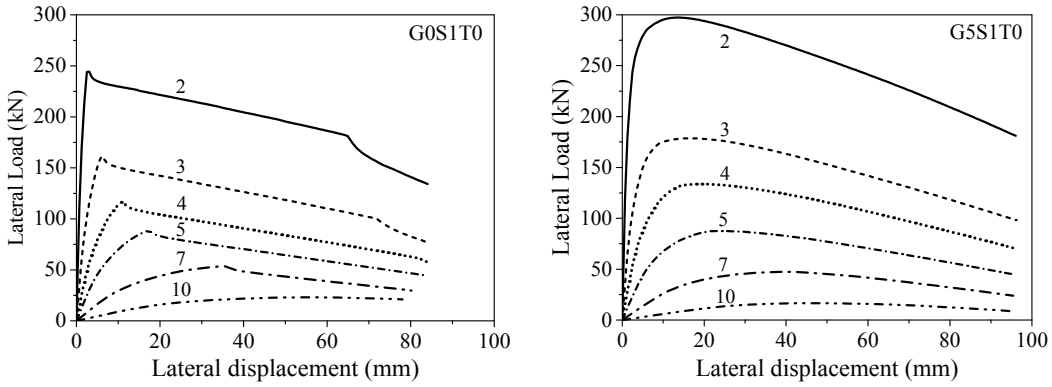

Fig. 19 Influence of shear-span ratio on FRP-steel confined RC columns

Fig.20

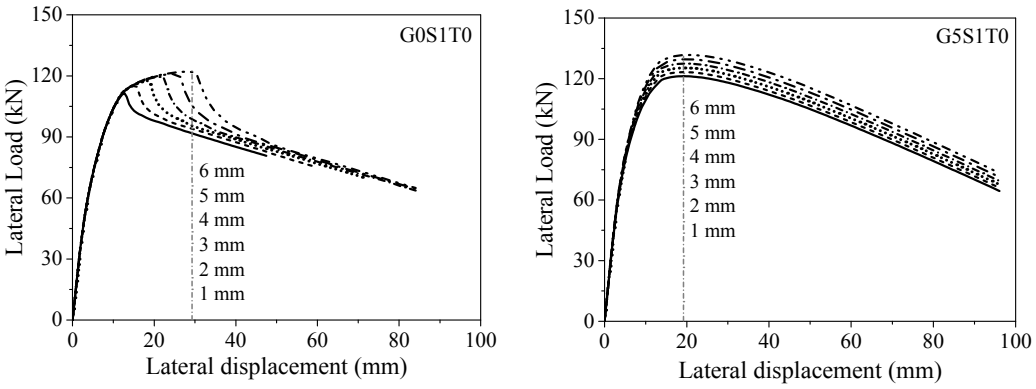

Fig. 20 Effects of steel tube thickness on FRP-steel confined RC columns

Fig.21

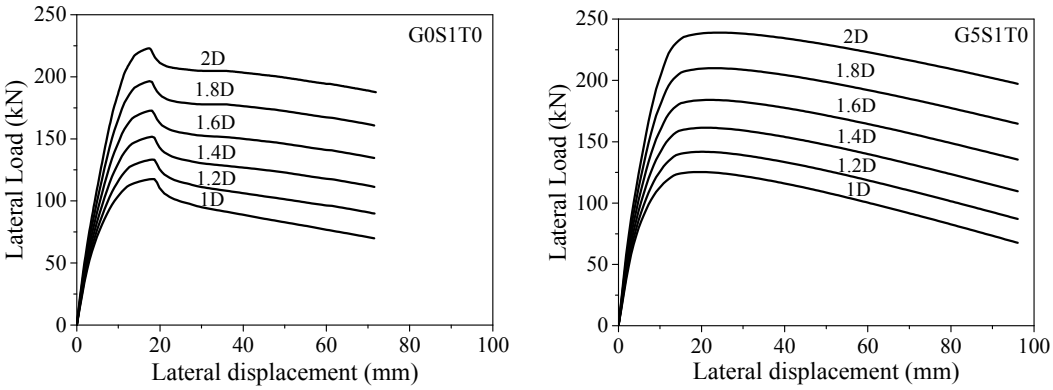

Fig. 21 Effects of longitudinal bars ratio on FRP-steel confined RC columns

Fig.22

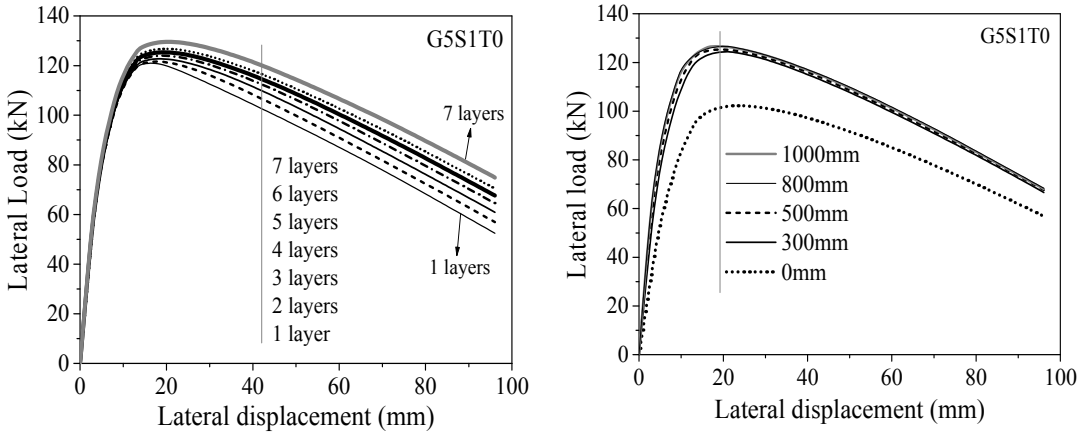

Fig. 22 Effects of confining layer number and the height of GFRP on the confined columns

Fig.23

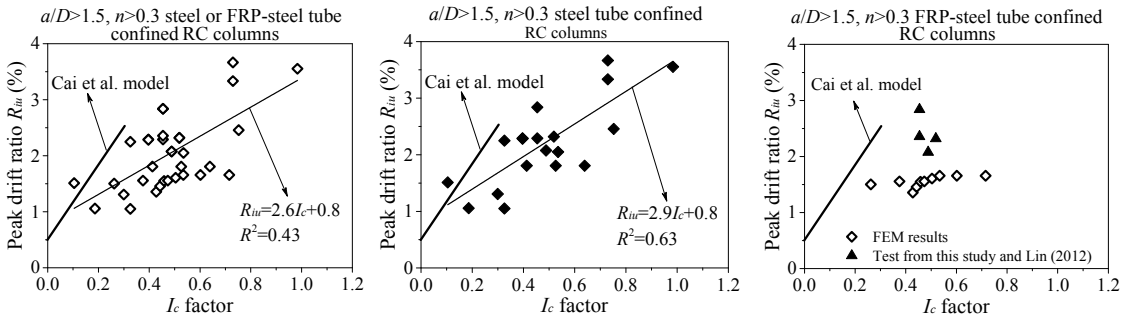

Fig.23 Relationship between peak drift ratio and I_c factor of confined RC columns